AE-70-023-8

THE UNIVERSITY OF TENNESSEE

DEPARTMENT OF MECHANICAL
AND AEROSPACE ENGINEERING

RAREFIED–GAS VISCOSEAL

by

HARVEY J. WILKERSON

August 1970

Knoxville, Tennessee 37916

AE-70-023-8

The University of Tennessee

Department of Mechanical and Aerospace Engineering

RAREFIED-GAS VISCOSEAL
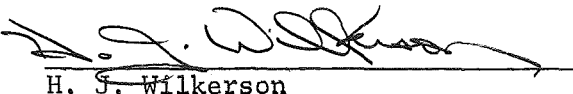
by

HARVEY J. WILKERSON

August 1970

Knoxville, Tennessee 37916

FOREWORD

This document is submitted as an interim report on the rarefied-gas viscoseal investigation which is a portion of "A Fundamental Study in Low-Density Gas Dynamics" at the University of Tennessee. Support for this work was provided by the National Aeronautics and Space Administration under Research Grant 43-001-023. These studies, under the direction of Dr. M. W. Milligan, have been confined to internal rarefied gas dynamics and have, in addition to the viscoseal, included investigations of low density flows in long and short cylindrical tubes, annuli, porous media, long square tubes, and nozzles.

This report was submitted to the University of Tennessee in partial fulfillment of the requirements for the degree of Doctor of Philosophy and is presented here with minor changes in format.

Approved: *M. W. Milligan*   *H. J. Wilkerson*
          M. W. Milligan   H. J. Wilkerson
          Principal Investigator

i

ABSTRACT

A fundamental study of the rarefied-gas viscoseal was initiated to expand the basic understanding of its operation under low-density conditions. The efforts reported consist of both experimental and analytical investigations. The theoretical analyses are based on formulating rarefied corrections to the laminar continuum equations for viscous flow. Both slip boundary conditions and self-diffusion contributions are applied to the Reynolds lubrication equations. An experimental investigation has been conducted on a multiple grooved two-inch diameter viscoseal over a wide range of gas densities and shaft speeds up to 30,000 rpm. Comparisons are presented between actual viscoseal performance and the theoretical predictions for both sealing coefficient and net leakage parameters as functions of the degree of gas rarefication. Comparisons with the experimental data of several other investigators are made.

In general the developed theoretical models predict the trends of the experimental data; however, some deviations between the theories and experiment exist.

TABLE OF CONTENTS

LIST OF TABLES

LIST OF FIGURES

LIST OF SYMBOLS

a	Axial land width
A	Groove cross sectional area
AR	Groove aspect ratio, b'/h
A_m	Manometer cross section area
b	Axial groove width
b'	Groove normal width, $b \cos \alpha$
c	Radial clearance
$\bar{c}$	Mean radial clearance
C_1, C_2, C_3, C_4	Constants of integration
C_5, C_6	Seal geometric constants
D	Shaft diameter
G	Slip coefficient constant of proportionality
h	Groove depth
H	Manometer total deflection
H_1, H_2	Manometer deflections
i, j, k	Counting indices
K	Boltzmann constant
ℓ	Groove length along helix angle
L	Seal axial length
m	Sealant mass per molecule
$\dot{m}$	Sealant mass flow rate
M	Sealant molecular weight
n	Molecular density, N/V

n_ℓ	Number of thread lands in seal section
N	Number of molecules
$\dot{N}$	Sealant molecular flow rate
N_K	Knudsen number, λ/c
N_{Kg}	Groove Knudsen number, λ/b'
N_s	Number of groove starts
P	Pressure
$\bar{P}$	Mean test section pressure
P_o	Atmospheric pressure
P_T	Upstream seal pressure
P_b	downstream seal pressure
ΔP	Differential pressure across seal, $P_T - P_b$
Q	Sealant volumetric flow rate
r	Coordinate distance
rr	Coordinate distance
r_1	Inner radius of annulus (shaft)
r_2	Outer radius of annulus (housing)
r_p	Seal pressure ratio, P_T/P_b
r_t	Tube radius
r_H	Hydraulic radius
R	Distance ratio, r/b'
RR	Distance ratio, rr/b'
Re_c	Clearance Reynolds number, $\rho Uc/\mu$
R_o	Universal gas constant
S	Elemental area

t	Tangent of helix angle α
Δt	Flow measurement time increment
T	Absolute temperature
u,v,w	Velocity components in ξ, η, z coordinates
$\bar{u}$	Average rotor induced velocity, King's analysis
U	Surface velocity
V	Volume
$\bar{V}$	Mean molecular speed
V_o	Calibrated volume
W	Manometer fluid specific weight
x,y,z	Coordinates
α	Helix angle
β	Seal geometric parameter, $(h + c)/c$
γ	Seal geometric parameter, $b/(a + b)$
δ	Flow ratio, King's analysis
ϵ	Distance
ζ	Coefficient of slip
η, ξ	Coordinates
θ	Angle
λ	Mean free path
μ	Viscosity
μHg	Micron of mercury pressure
ρ	Density
σ	Ratio of molecular collisions
τ	Elemental volume
ψ	Rarefied viscoseal parameter

ω	Solid angle
Ω	Angular velocity
Λ	Sealing Coefficient

Special Subscripts

r	Refers to land
g	Refers to groove
ξr	Refers to ξ direction in region of land
ηr	Refers to η direction in region of land
ξg	Refers to ξ direction in region of groove
ηg	Refers to η direction in region of groove
y	Refers to axial component

CHAPTER I

INTRODUCTION

Background

A fundamental study of the gas viscoseal was initiated to
expand the basic understanding of its operation under low density
conditions.

This investigation was a portion of "A Fundamental Study in Low-
Density Gas Dynamics" supported at the University of Tennessee by the
National Aeronautics and Space Administration under Research Grant
43-001-023. These studies, under the direction of Dr. M. W. Milligan,
have been confined to internal rarefied gas dynamics and have, in
addition to the viscoseal, included investigations of low density flows
in long and short cylindrical tubes, annuli, porous media, long square
tubes, and nozzles.

A viscoseal is a dynamic shaft seal which consists of essentially
two elements, a shaft and a housing around it. Helical grooves are provided
on the shaft and/or the housing,and the relative motion of these two
surfaces produces a viscous pumping action on the fluid in the grooves.

The viscoseal is normally designed with minimal clearance in the
annular space between the shaft and the housing to maximize the performance.
Since this seal does not depend on physical contact to provide sealing
action, it offers essentially zero wear rates and the possibility of low

1

leakage rates. Figure 1 shows a typical viscoseal with a grooved shaft and a smooth housing.

Mechanical devices which embody the viscoseal geometry are of early origin and have been in use in excess of 100 years in several applications. These include uses as a screw extruder for producing flow of very viscous liquids or plastics, screw oil pumps, and as shaft sealing devices. The history of these developments into the present day viscoseal is well presented in References [1,2, and 3][1]. The primary stimuli for the recent renewed interest in the viscoseal have been the demands for advanced sealing concepts in the space and nuclear programs. Most of the recent viscoseal investigations have been primarily concerned with liquids as the sealant with emphasis on the continuum regimes including both laminar and turbulent flow. The requirement of restricting the flow of fluids to a space environment has necessitated the development of seals which operate in the rarefied-gas flow regime. As the leakage fluid passes through the seal system, its character changes from that of a continuum fluid at the higher density end to that of a rarefied fluid at the lower density end where the fluid exits to space. The complete seal system would include several components and elements of different design and purpose depending on whether the fluid being handled was a liquid, a gas at continuum conditions, a rarefied gas or a combination of these. This study is concerned with the last element in the total seal system just prior to the fluid exiting to space as a rarefied gas.

---

[1]Numbers in brackets refer to similarly numbered references in the Bibliography.
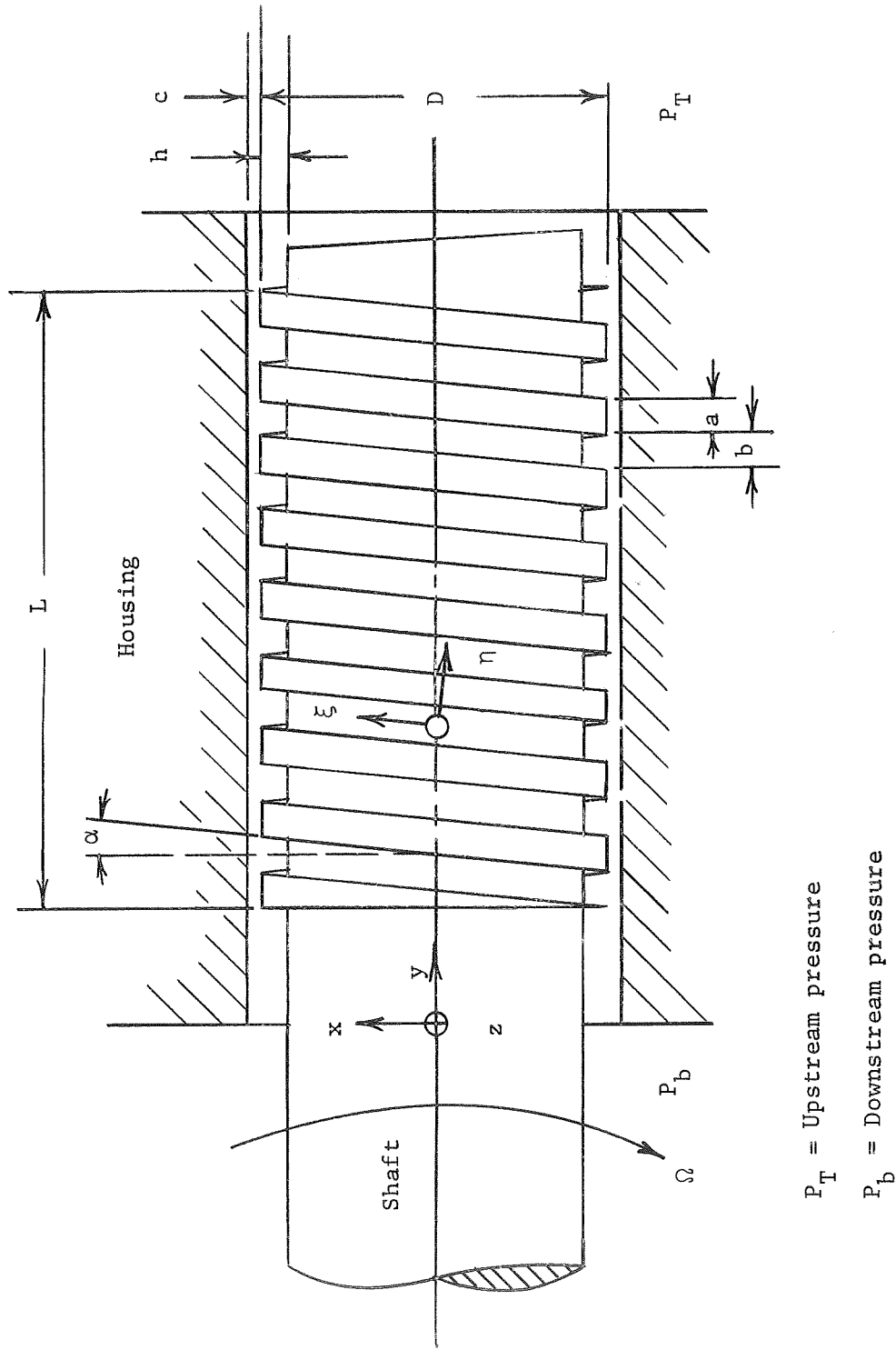
Figure 1. Basic Elements of the Viscoseal.

P_T = Upstream pressure

P_b = Downstream pressure

Flow of a rarefied gas is characterized by the ratio of the mean free path, λ, to the significant dimension of the flow field. A gas under this condition does not behave entirely as a continuous fluid but also exhibits some characteristics of its coarse molecular structure. The dimensionless parameter Knudsen number, which is the ratio of λ to the characteristic system dimension, is a measure of the degree of rarefication. When the Knudsen number is quite small, i.e., less than 0.01, then λ is small in comparison to the flow system characteristic dimension, and therefore intermolecular collisions are predominant over collisions with the boundaries. Here one is concerned with macroscopic motion of the gas as a continuum rather than the microscopic motion of the individual molecules. The concepts of classical gas dynamics apply to this flow situation. For flows in which the value of the Knudsen number is large, i.e., greater than 10, collisions with the boundaries dominate over collisions between molecules. This class of fluid transport is commonly defined as "free molecular flow." The region between the continuum and the free molecular regimes is commonly termed "slip flow." A broad range of flow of varying character may exist in this region depending on the proximity of the gas to the continuum or the free molecular regions. As the gas becomes rarefied, the intermolecular momentum transport in the vicinity of the walls diminishes due to the reduced number of inter-molecular collisions. This action produces an apparent diminution in the viscosity of the gas and creates the effect of a finite "slip velocity" in portions of the fluid adjacent to the walls. Hence originates the term "slip flow."

Relatively few experimental investigations have been devoted to rarefied-gas viscoseals. Baron [4] performed experiments using air and hydrogen as the sealants, but his data are well within the continuum regime. Hodgson [5] performed experiments with mercury vapor as the sealant, but reports only a limited amount of data. King [6] performed tests using air, argon, helium, and sulfur hexafluoride gas, and a portion of these data are noteworthy in being in the non-continuum regime. The efforts of King are discussed in more detail in Appendix B. Hodgson and Milligan [7] obtained viscoseal data for air, but again these were in the continuum regime.

The theoretical analyses of viscoseals having a rarefied gas as the sealant are also very limited. King [6] performed a theoretical analysis using a simplified model for the rotor induced flow in the grooves and a modified form of the Poiseuille viscous flow tube equation for the pressure induced flows. King's analysis is discussed in detail in Appendix B. Hodgson [5] performed an analysis of the viscoseal from the continuum region to the free molecular regimes by considering individually the pressure induced flows in the grooves and the clearance annulus superimposed with the rotor induced flow in the grooves. The procedure used is patterned after the work of Knudsen in formulating equations of a certain form to match the molecular and continuum limits. The analysis of Hodgson is currently under investigation by a fellow researcher, Mr. K. E. Patterson, and will be documented in the forthcoming master's thesis [8].

Statement of the Problem

This study is a combined experimental and analytical investigation
of a visco-type gas seal operating under rarefied flow conditions. The
experimental investigations include the gathering of performance data on
a multiple grooved two-inch diameter viscoseal over a wide range of shaft
speeds and gas densities. The theoretical analyses are based on
formulating "rarefied" corrections to the laminar continuum equations for
viscous flow. It is necessary to account for the slip velocity at the
walls and to account for the molecular diffusion which occurs due to the
concentration gradient. In the analyses the flow is assumed steady,
isothermal, and laminar. The sealant fluid is considered to be of
constant viscosity, Newtonian, and a monatomic gas which obeys the perfect
gas equation of state.

CHAPTER II

THEORETICAL ANALYSES

The analysis of the flow in a viscoseal geometry presents a difficult
and complex problem regardless of the flow regime in question. The
inclusion of rarefication effects further enlarges the difficulties through
the increased complexity of the boundary conditions in addition to the
usual need for numerical integration if diffusion effects are included.
The analysis approach selected has been one of formulating "rarefied"
corrections to the laminar continuum equations for viscous flow in the
viscoseal. This approach is similar to that of several previous
investigations [9, 10, 11, 12, 13, and 14] of internal rarefied flow that
have indicated that a single model for gas flow through tubes and annuli,
applicable to the flow regimes extending from continuum to molecular flow,
can be derived by the inclusion of rarefied effects on the continuum
model. Weber [9] developed a rather complete theory of rarefied gas flow
through long tubes by combining the flow predicted from the continuum
equation using slip boundary conditions with diffusion flow which exists
due to a concentration gradient. Milligan experimentally verified the
analysis technique of Weber for rarefied flow in long tubes [10] with
excellent agreement. The superposition analysis technique was extended
to include long annuli by Milligan, Cowling, and Wilkerson [12, 13, and
14] with continuing success.

In 1959 Boon and Tal published [15] a significant analysis of the
viscoseal in the laminar continuum regime for a constant density fluid.

The viscoseal geometry was approximated by two flat plates, one of which was grooved, moving parallel to each other. The flow field was developed from a superposition of Couette flows along and across the grooves. The resulting velocity distributions were integrated to obtain the volumetric flow rate, and the pressure generation for zero net leakage conditions was developed. Subsequent investigations by Stair [16, 17, 18, and 19] using liquids as the sealant showed very good agreement with the analysis of Boon and Tal. The data of Hodgson and Milligan [7] using air as the sealant also substantiated this analysis for laminar continuum operation with gases.

In the work presented here the analysis of Boon and Tal has been selected as the model for predicting the laminar continuum viscous flow. This model will serve as the basis for obtaining two different but closely related non-continuum solutions. The first of these rarefied solutions will be derived by the application of slip boundary conditions to obtain a closed form solution referred to as the "slip-modified Reynolds solution." A second more complex solution will be obtained using the analysis technique of Weber to combine the continuum flow plus the slip flow contribution modified for the molecules which do not experience slip boundary conditions plus the self-diffusion flows. The second solution will be referred to as the "composite solution."

Slip-Modified Reynolds Solution

Consider a screw formed on a shaft located concentrically within a cylindrical housing with a radial clearance c. The annular space is filled with a gas and the shaft is moving relative to the housing with an

angular velocity, Ω. Figure 2 shows a developed view of the viscoseal geometry. The (x, y) axes are along and normal to the direction of relative motion and the (ξ, η) axes are parallel and normal to the grooves. The (x, y) and (ξ, η) coordinates systems are related by:

$$\xi = x \cos \alpha + y \sin \alpha$$

$$\eta = y \cos \alpha - x \sin \alpha.$$

Previous investigators [15, 16] have reduced the describing partial differential momentum equations to the Reynolds lubrication equations. These analyses were based on the flat plate model of Figure 2 and assumed steady, isothermal, two-dimensional, laminar flow. Further, these analyses assumed inertia forces to be negligible in comparison to viscous forces and neglected body forces and end effects. The describing mathematical model is taken as:

$$\frac{d^2 u}{dz^2} = \frac{1}{\mu} \frac{\partial P}{\partial \xi} \tag{2-1}$$

$$\frac{d^2 v}{dz^2} = \frac{1}{\mu} \frac{\partial P}{\partial \eta}. \tag{2-2}$$

Integration of (2-1) and (2-2) gives:

$$u = \frac{1}{2\mu} \frac{\partial P}{\partial \xi} z^2 + C_1 z + C_2 \tag{2-3}$$

$$v = \frac{1}{2\mu} \frac{\partial P}{\partial \eta} z^2 + C_3 z + C_4. \tag{2-4}$$

The integration constants are determined by the boundary conditions. To account for the non-continuum effects, slip boundary conditions are introduced as derived by Kennard [20]. For a monatomic gas, flowing within
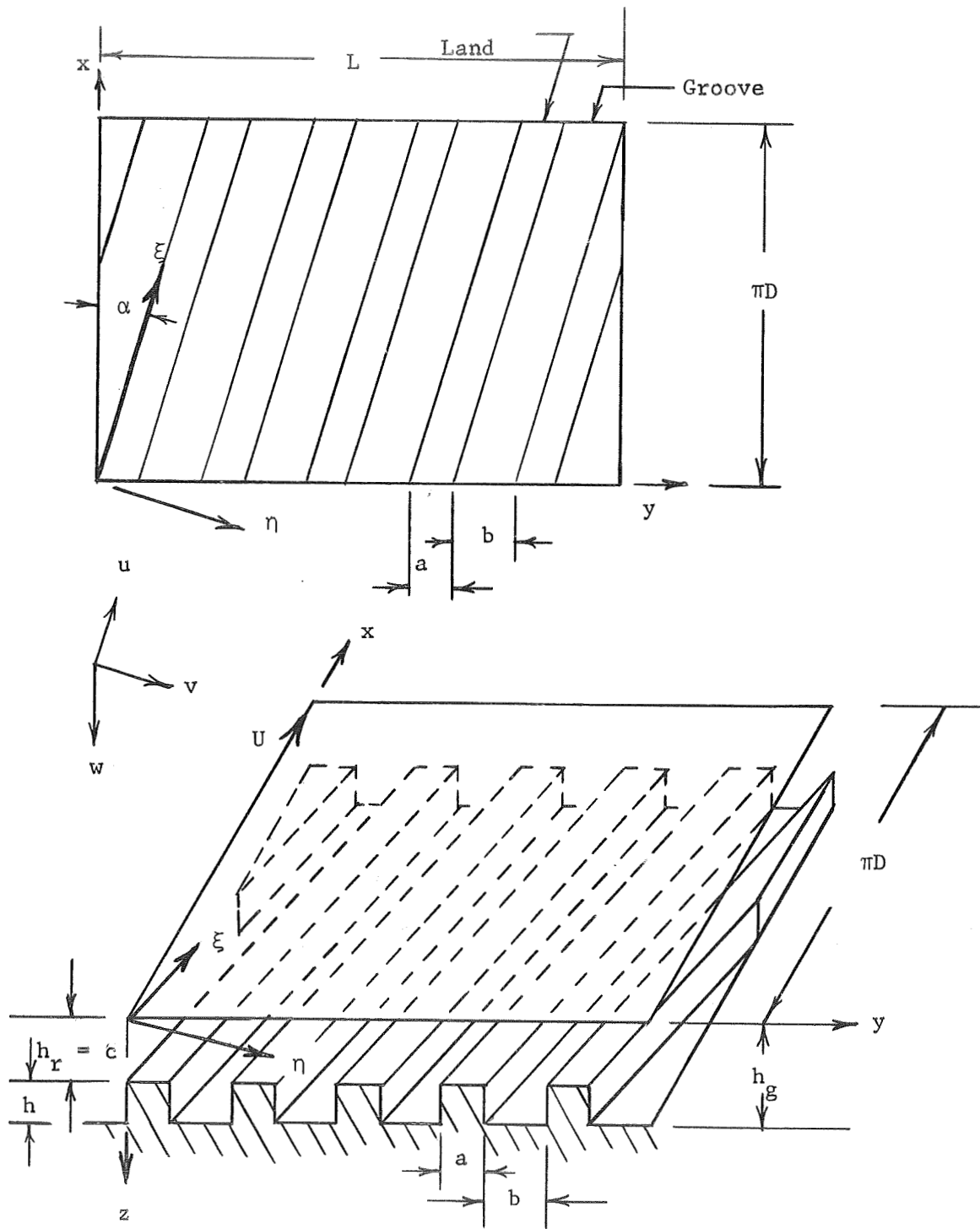
Figure 2. Developed Viscoseal Geometry.

two parallel boundaries, the slip boundary condition can be written

in the following general form:

$$u_{gas}\Big|_{z=0} = u_{wall} + G\lambda\left(\frac{\partial u}{\partial z}\right)\Big|_{z=0} + \frac{3}{4}\frac{\mu}{\rho T}\left(\frac{\partial T}{\partial x}\right)\Big|_{z=0} + O(\lambda^2), \qquad (2\text{-}5)$$

where u is the velocity in the tangential x direction, z is the direction

normal to the motion, and G is a proportionality constant. If the

temperatures of the surfaces are assumed constant and equal to the gas

temperature then the slip boundary condition reduces in general form to

$$u_{gas} = u_{wall} + G\lambda\left(\frac{\partial u}{\partial z}\right)_{z=0}. \qquad (2\text{-}6)$$

For the particular geometry under study, the slip boundary conditions

are:

Along the lands:

$$u_r\Big|_{z=0} = U\cos\alpha + G\lambda\frac{du_r}{dz}\Big|_{z=0} \equiv u_1$$

$$u_r\Big|_{z=h_r} = -G\lambda\frac{du_r}{dz}\Big|_{z=h_r} \equiv u_2$$

Along the groove:

$$u_g\Big|_{z=0} = U\cos\alpha + G\lambda\frac{du_g}{dz}\Big|_{z=0} \equiv u_3$$

$$u_g\Big|_{z=h_g} = -G\lambda\frac{du_g}{dz}\Big|_{z=h_g} \equiv u_4.$$

Across the lands:

$$v_r\Big|_{z=0} = -U\sin\alpha + G\lambda\frac{dv_r}{dz}\Big|_{z=0} \equiv v_1$$

$$v_r \Big|_{z = h_r} = - G\lambda \frac{dv_r}{dz} \Big|_{z = h_r} \equiv v_2.$$

Across the groove:

$$v_g \Big|_{z = 0} = - U \sin \alpha + G\lambda \frac{dv_g}{dz} \Big|_{z = 0} \equiv v_3$$

$$v_g \Big|_{z = h_g} = - G\lambda \frac{dv_g}{dz} \Big|_{z = h_g} \equiv v_4.$$

Using the above boundary conditions the following velocity components are determined:

Along the lands:

$$u_r = \frac{1}{2\mu} \frac{\partial P}{\partial \xi} (z^2 - h_r z) + \left(\frac{u_2 - u_1}{h_r}\right) z + u_1. \qquad (2\text{-}7)$$

Along the grooves:

$$u_g = \frac{1}{2\mu} \frac{\partial P}{\partial \xi} (z^2 - h_g z) + \left(\frac{u_4 - u_3}{h_g}\right) z + u_3. \qquad (2\text{-}8)$$

Across the lands:

$$v_r = \frac{1}{2\mu} \frac{\partial P}{\partial \eta} (z^2 - h_r z) + \left(\frac{v_2 - v_1}{h_r}\right) z + v_1. \qquad (2\text{-}9)$$

Across the grooves:

$$v_g = \frac{1}{2\mu} \frac{\partial P}{\partial \eta} (z^2 - h_g z) + \left(\frac{v_4 - v_3}{h_g}\right) z + v_3. \qquad (2\text{-}10)$$

The slip velocities at the walls can now be determined, and the following velocity distribution equations obtained:

$$u_r = \frac{1}{2\mu}\frac{\partial P}{\partial \xi}(z^2 - h_r z) + \left(\frac{-U\cos\alpha}{1 + 2G\lambda/h_r}\right)\frac{z}{h_r}$$

$$+ U\cos\alpha\left(\frac{1 + G\lambda/h_r}{1 + 2G\lambda/h_r}\right) - \frac{1}{2\mu}\frac{\partial P}{\partial \xi}h_r^2\frac{G\lambda}{h_r} \qquad (2-11)$$

$$u_g = \frac{1}{2\mu}\frac{\partial P}{\partial \xi}(z^2 - h_g z) + \left(\frac{-U\cos\alpha}{1 + 2G\lambda/h_g}\right)\frac{z}{h_g}$$

$$+ U\cos\alpha\left(\frac{1 + G\lambda/h_g}{1 + 2G\lambda/h_g}\right) - \frac{1}{2\mu}\frac{\partial P}{\partial \xi}h_g^2\frac{G\lambda}{h_g} \qquad (2-12)$$

$$v_r = \frac{1}{2\mu\partial\eta}\frac{\partial P}{}(z^2 - h_r z) + \left(\frac{U\sin\alpha}{1 + 2G\lambda/hr}\right)\frac{z}{h_r}$$

$$- U\sin\alpha\left(\frac{1 + G\lambda/h_r}{1 + 2G\lambda/h_r}\right) - \frac{1}{2\mu\partial\eta}\frac{\partial P}{}h_r^2\frac{G\lambda}{h_r} \qquad (2-13)$$

$$v_g = \frac{1}{2\mu}\frac{\partial P}{\partial \eta}(z^2 - h_g z) + \left(\frac{U\sin\alpha}{1 + 2G\lambda/h_g}\right)\frac{z}{h_g}$$

$$- U\sin\alpha\left(\frac{1 + G\lambda/h_g}{1 + 2G\lambda/h_g}\right) - \frac{1}{2\mu\partial\eta}\frac{\partial P}{}h_g^2\frac{G\lambda}{h_g}. \qquad (2-14)$$

Noting that the axial velocity components are:

$$u_y = u\sin\alpha \qquad (2-15)$$

$$v_y = v\cos\alpha \qquad (2-16)$$

the axial flow rate components $Q_{\xi r}$, $Q_{\xi g}$, $Q_{\eta r}$ and $Q_{\eta g}$ may be determined. The width of the flow path for the ξ land flow component is $(1 - \gamma)\pi D$ and the path width for the ξ groove flow is $\gamma\pi D$. The ratio of the groove

width to the groove plus land width is defined as γ. The axial component of the ξ coordinate land flow is:

$$Q_{\xi r} = (1 - \gamma)\pi D \int_0^{h_r} U_{ry} dz = (1 - \gamma)\pi D \int_0^{h_r} U_r \sin \alpha \, dz \ . \tag{2-17}$$

Substituting Equation (2-11) into Equation (2-17) and integrating gives

$$Q_{\xi r} = (1 - \gamma)\pi D \sin \alpha [\frac{1}{2\mu} (\frac{\partial P}{\partial \xi})_r h_r^3 (- \frac{G\lambda}{h_r} - \frac{1}{6}) + U \cos \alpha \frac{h_r}{2}] \ . \tag{2-18}$$

In a similar manner:

$$Q_{\xi g} = \gamma \pi D \sin \alpha [\frac{1}{2\mu} (\frac{\partial P}{\partial \xi})_g h_g^3 (- \frac{G\lambda}{h_g} - \frac{1}{6}) + U \cos \alpha \frac{h_g}{2}] \tag{2-19}$$

$$Q_{\eta r} = (1 - \gamma) \pi D \cos \alpha [\frac{1}{2\mu} (\frac{\partial P}{\partial \eta})_r h_r^3 (- \frac{G\lambda}{h_r} - \frac{1}{6}) - U \sin \alpha \frac{h_r}{2}] \tag{2-20}$$

$$Q_{\eta g} = \gamma \pi D \cos \alpha [\frac{1}{2\mu} (\frac{\partial P}{\partial \eta})_g h_g^3 (- \frac{G\lambda}{h_g} - \frac{1}{6}) - U \sin \alpha \frac{h_g}{2}] \ . \tag{2-21}$$

The pressure gradients in Equations (2-18) through (2-21) may be replaced by the more convenient axial gradients by noting that

$$\frac{\partial P}{\partial \xi} = \frac{\partial P}{\partial y} \sin \alpha \ , \tag{2-22}$$

and

$$(1 - \gamma) (\frac{\partial P}{\partial \eta})_r + (\frac{\partial P}{\partial \eta})_g = \frac{\partial P}{\partial y} \cos \alpha \ . \tag{2-23}$$

From the continuity of mass, the flow across the groove in the η direction must equal the flow across the land in this direction. Thus it can be shown that

$$[\frac{1}{2\mu} (\frac{\partial P}{\partial \eta})_r \, h_r^3 \, (- \frac{G\lambda}{h_r} - \frac{1}{6}) - U \sin \alpha \, \frac{h_r}{2}] =$$

$$[\frac{1}{2\mu} (\frac{\partial P}{\partial \eta})_g \, h_g^3 (- \frac{G\lambda}{h_g} - \frac{1}{6}) - U \sin \alpha \, \frac{h_g}{2}]. \qquad (2-24)$$

The total flow is given by:

$$Q = Q_{\xi r} + Q_{\xi g} + Q_{\eta r} + Q_{\eta g}. \qquad (2-25)$$

Using Equations (2-18) through (2-25), the expression for the axial flow is:

$$Q = - \frac{1}{12\mu} \frac{\partial P}{\partial y} \frac{c^3 \pi D}{(1 + t^2)} \, [t^2 (1 - \gamma)(1 + \frac{6G\lambda}{c}) + (1 + \frac{6G\lambda}{\beta c})(\beta^3)(\gamma t^2 + \frac{1}{\psi})]$$

$$+ \frac{Uc\pi D}{2} \, \frac{t(1 - \gamma)(\beta - 1)}{1 + t^2} [\frac{\beta^3 (1 + \frac{6G\lambda}{\beta c})}{\psi(1 + \frac{6G\lambda}{c})} - 1], \qquad (2-26)$$

where

$$\beta = \frac{h + c}{c}$$

$$\gamma = \frac{b}{a + b}$$

$$\psi = (1 - \gamma)\beta^3(\frac{1 + \frac{6G\lambda}{\beta c}}{1 + \frac{6G\lambda}{c}}) + \gamma$$

$$t = \tan \alpha$$

The Knudsen number for the viscoseal is defined as

$$N_K \equiv \frac{\lambda}{c} , \qquad (2-27)$$

where seal radial clearance, c, has been selected as the characteristic system dimension because of the manner of its appearance in Equation (2-26) in relation to the mean free path λ.

Letting

$$f_1(N_K) = t^2(1-\gamma)(1+6GN_K) + (1 + \frac{6GN_K}{\beta})(\beta^3)(\gamma t^2 + \frac{1}{\psi}),$$

and

$$f_2(N_K) = t(1-\gamma)(\beta-1)[\frac{\beta^3(1+\frac{6GN_K}{\beta})}{\psi(1+6GN_K)} - 1],$$

Equation (2-26) becomes

$$Q = -\frac{1}{12\mu}\frac{\partial P}{\partial y}\frac{c^3\pi D}{(1+t^2)}f_1(N_K) + \frac{Uc\pi D}{2(1+t^2)}f_2(N_K). \tag{2-28}$$

The most useful situation for the viscoseal as a sealing device would be to have Q equal to zero. Taking $Q = 0$ and $\frac{\partial P}{\partial y} \sim \frac{\Delta P}{L}$, the sealing coefficient is defined and evaluated from Equation (2-28) as

$$\Lambda \equiv \frac{6\mu UL}{\Delta P c^2} = \frac{f_1(N_K)}{f_2(N_K)}. \tag{2-29}$$

Further consideration now needs to be given to the slip coefficient constant of proportionality "G". Various investigators have developed expressions for this proportionality constant ranging from 2/3 [21] to (2 - f)/f [20] where f is the fraction of their tangential momentum which molecules give up upon striking a solid boundary. Published values of f by Kennard [20] range from 0.79 for air flowing over fresh shellac to 1.00 for air or CO_2 over machined brass. A value of f equal to one is taken to be realistic for the flow of gases over machined surfaces. Thus the value of the slip coefficient G was taken to be unity.

Knudsen number as defined in Equation (2-27) indicates the degree of rarefication since it becomes large as the mean free path, λ, becomes

large. When the Knudsen value value becomes small and approaches zero, corresponding to continuum conditions, then Equation (2-29) reduces to the continuum, no slip, solution shown by Stair [16].

$$\Lambda_{cont.} = \frac{\beta^3(1 + t^2) + \gamma t^2(1 - \gamma)(\beta^3 - 1)^2}{\gamma t(1 - \gamma)(\beta^3 - 1)(\beta - 1)} .$$ (2-30)

Correction for the Particles Which Do Not
Experience Slip Boundary Conditions

In the previous section where the slip-modified Reynolds solution was derived, slip boundary conditions were applied to account for the decreased intermolecular momentum transport at the walls. The analysis attributed a slip velocity relative to the walls for all the molecules adjacent to these surfaces. For the case of stationary walls, this implies that every molecule, on the average, will possess additional flow velocity due to the slip flow contribution. The preponderance of evidence presented by Weber [9], Kennard [20], Present [21], and Fryer [22] indicate that molecules whose last collision was at the wall can have no slip velocity since such molecules are diffusely reflected from the walls. Thus only those molecules coming from collisions with other molecules can possess a slip velocity. A correction will now be developed to account for those molecules which do not experience slip boundary conditions due to their collisions with the walls. The correction will be established by determining the ratio of the molecule-to-molecule collisions to the total number of collisions, or the sum of the molecule-to-wall plus the molecule-to-molecule collisions. This ratio, σ, represents the fraction of molecules present which experience the slip boundary condition.

The number of molecules striking the wall per unit time and unit area is [21]

$$\frac{n\overline{V}}{4}$$

where $\overline{V}$ is the mean molecular speed. If one considers the unwrapped viscoseal geometry of Figure 2, page 10, the seal surface area is approximated by

$$2\pi DL + 2h \frac{\pi D}{\cos \alpha} \frac{L}{(a + b)} ,$$

where the right hand term is the surface area contributed by the groove side walls. Thus the number of molecule-to-wall collisions in unit time is

$$\frac{n\overline{V}}{2} \pi DL[1 + \frac{h}{\cos \alpha(a + b)}].$$

The total number of molecule-to-molecule collisions per unit time and unit volume is [21]

$$\frac{n\overline{V}}{\lambda} .$$

The volume of the viscoseal is the volume of the annular space plus the volume of the grooves. Thus the total number of molecule-to-molecule collisions per unit time is

$$\frac{n\overline{V}}{\lambda} [\pi L(r_2^2 - r_1^2) + \frac{\pi DL \cdot h \cdot b}{(a + b)}].$$

Since

$$(r_2^2 - r_1^2) = (r_2 + r_1)(r_2 - r_1),$$

and, due to the small clearance of the normal viscoseal geometry,

$$r_1 + r_2 \sim D$$

and

$$r_2 - r_1 = c,$$

then the expression simplifies to

$$\frac{n\overline{V}}{\lambda} \pi DL \left[c + \frac{h \cdot b}{a + b}\right].$$

Hence, the proportion of the molecules which experience slip is

$$\sigma = \frac{1/N_K \left[1 + \gamma(\beta - 1)\right]}{1/N_K[1 + \gamma(\beta - 1)] + \frac{1}{2}[1 + \frac{h}{\cos \alpha(a + b)}]} \quad , \tag{2-31}$$

with

$$\beta \equiv \frac{h + c}{c} \qquad \gamma \equiv \frac{b}{a + b}$$

$$N_K \equiv \frac{\lambda}{c} \qquad \text{and} \qquad \frac{h}{c} = (\beta - 1).$$

In the solution of the slip-modified Reynolds equation, it will be recalled that boundary conditions were not specified on the groove side walls. Thus it is more in keeping with the manner of the analysis to omit the molecule-to-wall collisions which occur on these surfaces and contribute the $h/\cos \alpha(a + b)$ term in the denominator of Equation (2-31). With this restriction, the equation becomes

$$\sigma = \frac{1}{1 + N_K/2[1 + (\beta - 1)\gamma]} \quad . \tag{2-32}$$

In the analysis of slip flow through long tubes by Weber [9], Fryer[22], and Milligan [10], the resulting flow equation can be manipulated into two separate terms. One of these terms is the continuum

Poiseuille flow term while the second term is the slip flow contribution and results from application of the slip boundary conditions. Equivalent type terms were obtained by Milligan, Cowling, and Wilkerson [21] in the analysis of rarefied flow in a long concentric annulus. For both of these geometries, the correction for the particles which do not experience slip was made by multiplying the slip flow contribution by σ, since it is this uncorrected term which implies that all the molecules possess the additional slip velocity. Thus when σ is applied in this manner the resulting slip contribution term has been corrected for the particles which experience wall collisions and thus possess no slip velocity. In the analysis of the slip-modified Reynolds solution for the viscoseal, the resulting expression of Equation (2-28) does not permit a straight-forward separation into a continuum term plus a slip term. Hence, the flow contribution of the slip boundary condition is separated in the following manner. The total rarefied flow of Equation (2-28) can be expressed as

$$Q_{total} = Q_{cont.} + (Q_{rarefied} - Q_{cont.}), \qquad (2\text{-}33)$$

where $Q_{cont.}$ is the continuum flow only and $Q_{rarefied}$ is the slip-modified Reynolds solution flow of Equation (2-28). Thus the bracketed right hand term of Equation (2-33) is the slip flow contribution, and the correction for the particles which do not experience slip may be made as

$$Q = Q_{cont.} + \sigma(Q_{rarefied} - Q_{cont.}). \qquad (2\text{-}34)$$

The continuum flow term, $Q_{cont.}$, is obtained by taking the limit of Equation (2-28) as the Knudsen number approaches zero. The resulting expression from Equation (2-28) may be simplified to

$$Q_{cont.} = -\frac{1}{12\mu}\frac{\Delta P}{L}\frac{c^3\pi D}{(1+t^2)}[\frac{\gamma t^2(1-\gamma)(\beta^3-1)^2+\beta^3(1+t^2)}{\beta^3(1-\gamma)+\gamma}]$$

$$+\frac{Uc\pi D}{2(1+t^2)}[\frac{\gamma t(1-\gamma)(\beta^3-1)(\beta-1)}{\beta^3(1-\gamma)+\gamma}] \qquad (2-35)$$

and is identical to that presented by Stair [16]. Letting

$$C_5 = \frac{\gamma t^2(1-\gamma)(\beta^3-1)^2+\beta^3(1+t^2)}{\beta^3(1-\gamma)+\gamma} ,$$

and

$$C_6 = \frac{\gamma t(1-\gamma)(\beta^3-1)(\beta-1)}{\beta^3(1-\gamma)+\gamma} ,$$

then Equation (2-34) may be written as

$$Q = -\frac{1}{12\mu}\frac{\Delta P}{L}\frac{c^3\pi D}{(1+t^2)}[\sigma f_1(N_K)+C_5(1-\sigma)]$$

$$+\frac{Uc\pi D}{2(1+t^2)}[\sigma f_2(N_K)+C_6(1-\sigma)]. \qquad (2-36)$$

Defining

$$f_3(N_K) \equiv \sigma f_1(N_K)+C_5(1-\sigma),$$

and

$$f_4(N_K) \equiv \sigma f_2(N_K)+C_6(1-\sigma),$$

then

$$Q = -\frac{1}{12\mu}\frac{\Delta P}{L}\frac{c^3\pi D}{(1+t^2)}f_3(N_K)+\frac{Uc\pi D}{2(1+t^2)}f_4(N_K). \qquad (2-37)$$

In a similar manner to that of Equation (2-29), the sealing coefficient for the slip-modified Reynolds solution with corrections for particles which do not experience slip is

$$\Lambda = \frac{6\mu UL}{\Delta Pc^2} = \frac{f_3(N_K)}{f_4(N_K)} .$$

(2-38)

Specific Molecular Flow Rates

Quite often it is more desirable to express results in terms of molecular flow rates than in terms of volumetric flow rates as given in Equations (2-28) and (2-37). The molecular flow, $\dot{n}$, is

$$\dot{n} = Qn,$$

(2-39)

where n is the average molecular density defined by the perfect gas equation of state

$$n = \frac{\bar{P}}{KT},$$

(2-40)

with $\bar{P}$ being the average seal pressure. If one uses the Chapman relationship [20] to describe the mean free path corresponding to the average seal pressure, then Equation (2-27) can be written as

$$N_K = \frac{\lambda}{c} = \frac{\mu(2\pi \frac{R_o}{M} T)^{1/2}}{2\bar{P}c}$$

(2-41)

With the use of Equations (2-39), (2-40), and (2-41), the previous expressions for volumetric flow rate may be written in terms of the specific molecular flow per unit of pressure drop across the seal. Equation (2-28) for the slip-modified Reynolds solution with no correction due to particles which do not experience slip is

$$\frac{\dot{n}}{\Delta P} = \frac{Qn}{\Delta P} = - (\frac{\pi}{2mKT})^{1/2} (\frac{c^2\pi D}{N_K(1 + t^2)L})f_1(N_K)$$

$$+(\frac{r_p + 1}{r_p - 1}) \frac{U c \pi D}{4KT(1 + t^2)} f_2(N_K),$$

(2-42)

where the relationship that

$$\Delta P = 2\overline{P} \left(\frac{r_p - 1}{r_p + 1}\right), \tag{2-43}$$

has been written in terms of the pressure ratio, r_p, across the seal in the right hand term. Similarly, the specific leakage flow rate with the correction for the particles that do not experience slip is

$$\frac{\dot{n}}{\Delta P} = - \left(\frac{\pi}{2mKT}\right)^{1/2} \left(\frac{c^2 \pi D}{N_K (1 + t^2) L}\right) f_3(N_K)$$

$$+ \left(\frac{r_p + 1}{r_p - 1}\right) \frac{Uc\pi D}{4KT(1 + t^2)} f_4(N_K). \tag{2-44}$$

It should be noted that for a fixed seal geometry and a given gas at a specified temperature, the specific molecular flow rates of Equations (2-42) and (2-44) are functions only of Knudsen number, the speed U, and the viscoseal pressure ratio, r_p. As the pressure ratio becomes high, then $(r_p + 1)/(r_p - 1)$ approaches unity and the specific flow rate is a function of the speed and the Knudsen number only.

Self-Diffusion

The term diffusion, as used here, refers to the molecular transfer which occurs due to a concentration gradient. If the gas is a pure unmixed gas, then the diffusion is one of self-diffusion. In their work concerning low density flow of gases in a capillary, Pollard and Present [23] suggested that at low pressures the total transport can be described by the superposition of the diffusive transport and a drift component. In his study of flow through long tubes, Weber [9] applied

the idea of the superposition of a diffusive component, a slip contribution, and the viscous component. Weber demonstrated that his solution has the correct limiting values for continuum and free molecule flows and adequately describes Knudsen's data for long tubes [24]. Milligan experimentally verified, with excellent agreement, the analysis technique of Weber for rarefied flow in long tubes [10]. Lund and Berman [25] developed empirical relations for the flow and self-diffusion of gases in both long and short capillaries by the superposition of the diffusive and drift components. They developed an algebraic expression which permits the direct computation of the Weber diffusion coefficient at any pressure and thus avoided the numerical integration inherent in the Pollard and Present treatment of self-diffusion. Lund and Berman demonstrated the adequacy of their model for describing self-diffusion and flow in capillaries in addition to the flow between flat plates. Milligan, Cowling, and Wilkerson [12, 13, and 14] extended the superposition analysis technique of Weber to long annuli with continuing success.

In this section, the self diffusion flow in both the grooves and annular space of the viscoseal will be discussed and evaluated separately using the Pollard and Present treatment as applied by Weber.

Annular Space Self-Diffusion

The self-diffusion flow in the clearance space of the rarefied-gas viscoseal was obtained by considering this flow to be that of a concentric annulus. The molecular transfer was determined by evaluating the net number of molecules crossing a plane normal to the annulus. The evaluation was done by considering separately the molecules which

come from the outer and the inner walls with the grooved inner wall taken

as being smooth and of diameter D as shown in Figure 1, page 3. The

details of this derivation are presented in Reference [12] and the

procedure used was essentially that given by Weber [9] and is similar to

that presented in Appendix A for the self-diffusion in the grooves. The

following equations were numerically integrated to obtain the diffusion

contribution in the annular space:

$$\overset{\bullet}{N}_{\substack{\text{net outer} \\ \text{wall}}} = - 2\bar{V}\lambda \frac{dn}{dy} (r_2 - r_1)^2 \int_{R_1}^{R_2} \int_{0}^{\phi_o} \int_{0}^{\pi/2} (R) \cdot$$

$$\sin \theta \cos^2 \theta (1 - e^{-R/N_K}) \, dR' \, d\phi \, d\theta \qquad (2\text{-}45)$$

$$\overset{\bullet}{N}_{\substack{\text{net inner} \\ \text{wall}}} = - 2\bar{V}\lambda \frac{dn}{dy} (r_2 - r_1)^2 \int_{R_1}^{R_2} \int_{\phi_o}^{\pi} \int_{0}^{\pi/2} (R') \cdot$$

$$\sin \theta' \cos^2 \theta' (1 - e^{-R/N_K}) \, dR' \, d\phi \, d\theta'. \qquad (2\text{-}46)$$

The total self-diffusion flow in the annular space is the sum of

Equations (2-45 and 2-46) and may be arranged into specific molecular

flow rate form using

$$\frac{dn}{dy} = \frac{d}{dy} \left(\frac{P}{KT}\right) = \frac{1}{KT} \frac{dP}{dy} \sim \frac{1}{KT} \frac{\Delta P}{L}$$

and

$$\bar{V} = 2\left[\frac{2KT}{\pi m}\right]^{1/2}$$

to obtain

$$\frac{\overset{\bullet}{N}}{\Delta P} = - 4\left(\frac{2}{\pi m KT}\right)^{1/2} \frac{(r_2 - r_1)^3}{L} N_K [\text{SUM (O.W.)} + \text{SUM (I.W.)}], \qquad (2\text{-}47)$$

where SUM (O.W.) and SUM (I.W.) designates the numerical integration

of the integrals of Equations (2-45 and 2-46), respectively.

Groove Self-Diffusion

The self diffusion flow in the grooves of the shaft was obtained in a similar manner to that of the diffusive flow in the annular space. The flow in the groove was determined by considering this transport to be that of a long groove of rectangular cross section. This neglects any curvature effects of the helical groove and becomes increasingly in error as the groove dimensions become of the order of magnitude of the seal diameter. The development work of the numerical scheme is that primarily of Cowling and Swicegood [33] and is contained in Appendix A for the reader's convenience.

As shown in Appendix A, the groove diffusion flow involves the numerical solution of the following type of equation:

$$\dot{N} = - \frac{\overline{V} N_{Kg}}{2\pi} \frac{dn}{d\xi} \int_0^h \int_0^{b'} \int_0^h \int_0^\infty \{ \frac{(b' - \eta)b'}{r^5} (1 - e^{-R/N_{Kg}}) $$

$$+ \frac{\eta b'}{rr^5} (1 - e^{-RR/N_{Kg}}) \} \xi^2 \, dz'(d\eta dz d\xi), \qquad (2\text{-}48)$$

where

$$N_{Kg} = \frac{\lambda}{b'}$$

is the Knudsen number of the groove flow with the groove width, b', being taken as the characteristic dimension. Again

$$\overline{V} = 2 [\frac{2KT}{\pi m}]^{1/2}$$

and

$$\frac{dn}{d\xi} = \frac{d}{d\xi}(\frac{P}{KT}) = \frac{1}{KT} \frac{dP}{d\xi} \sim \frac{1}{KT} \frac{\Delta P}{\ell} ,$$

where ℓ is now the groove length. The relation between the length of one groove and the axial seal length is

$$\ell = \frac{1}{N_S} \frac{\pi D}{\cos \alpha} \frac{L}{(a + b)} = \frac{L}{\sin \alpha} \quad ,$$

where N_S is the number of grooves. For a multiple grooved shaft the total groove diffusion flow is N_S times the flow of a single groove. Thus the total specific molecular flow due to the diffusion is

$$\frac{\dot{N}}{\Delta P} = - \frac{N_S \sin \alpha}{\pi L} (\frac{2}{\pi m K T})^{1/2} [\text{SUM (Walls)}], \tag{2-49}$$

where SUM (Walls) designates the numerical integration of the integral terms of Equation (2-48) to include the total walls of the grooves, reference Appendix A, Equation (A-15).

The total specific molecular flow for the composite solution is obtained by adding the continuum solution plus the slip flow contribution after correction for the molecules which do not experience slip plus the self-diffusion flows in the annular space and the grooves. Thus

$$\frac{\dot{N}}{\Delta P})_{composite} = \text{Eq. (2-44) + Eq. (2-47) + Eq. (2-49).} \tag{2-50}$$

It should be noted in summating the flows that the contributions of each equation must be evaluated at the same physical gaseous state. In the development of the groove self-diffusion the Knudsen number, N_{Kg}, was based on the groove width, b', rather than the seal radial clearance, c. Thus the corresponding value of groove Knudsen number for a given clearance Knudsen number is

$$N_{Kg} = N_K (\frac{c}{b'}) . \tag{2-51}$$

CHAPTER III

EXPERIMENTAL INVESTIGATION

The purpose of the experimental investigation was to obtain reliable performance data of a rarefied-gas viscoseal and thereby permit an evaluation of the theoretical models. The investigation was conducted on a multiple grooved two-inch diameter viscoseal over a wide range of shaft speeds and gas densities. Data were obtained for both sealing coefficient performance (no leakage) as well as with net leakage flow. All rarefied data were obtained using argon as the sealing fluid.

Viscoseal Test Section

The experimental apparatus was designed to investigate viscoseal performance in the gas flow regime between continuum and free molecule flow.

The viscoseal test section, Figure 3, consists of an outer housing with its associated vacuum pumping system surrounding a rotating grooved shaft. The shaft is a hollow eight-inch cantilever extension of a high speed spindle shaft which is belt-driven through an intermediate spindle by a direct current motor. The drive system is capable of seal shaft speeds from zero to 35,000 rpm. The speed control for the motor is self-regulating and maintains a selected speed within $\pm$ 0.1 percent. Since the entire test section operates under vacuum, a rubbing contact graphite ring seal is provided where the rotating shaft penetrates the housing. The ring seal is a series B-103032, Type E, manufactured by
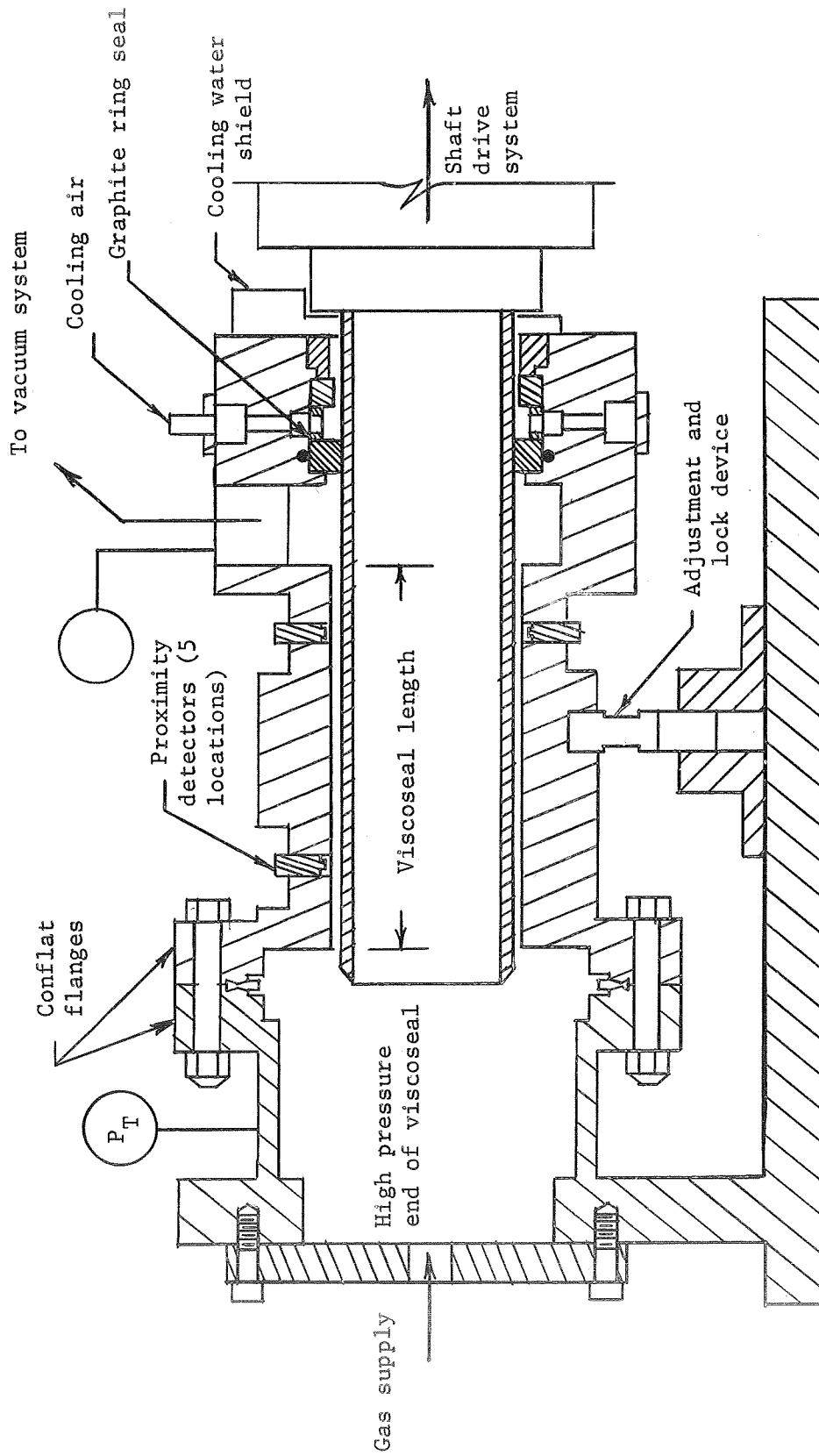
Figure 3. Viscoseal Test Section.

the Cleveland Graphite Bronze Division of the Clevite Corporation.
Cooling water and air are supplied at the ring seal end of the spindle
to minimize thermal growth due to the rubbing seal friction under
dynamic conditions. A Conflat vacuum flange is provided between the
housing and its support for purposes of sealing and to provide minor
adjustment capabilities for housing-shaft alignment. Other vacuum seals
are obtained by the use of "O" rings in addition to vacuum sealants for
threaded connections. The maintenance of a high quality vacuum system
with essentially no atmospheric leakage, except at the shaft seal, was
assured by the frequent use of a helium leak detector throughout the
experimental program.

All experimental data were obtained for a single viscoseal geometry
consisting of a grooved shaft inside a smooth housing. Pertinent
specifications of the rarefied viscoseal Number 1 are contained in
Table I.

A schematic diagram of the overall experimental test apparatus
is shown in Figure 4, page 32.

Vacuum Pumping System

It was necessary to develop a vacuum pumping system capable of
providing the desired low pressures and gas flow rates. This task was
accomplished by connecting two independent vacuum pumping systems in
parallel to a common reservoir, Figure 4. One of these pumping systems
consisted of a single stage rotary oil-sealed mechanical pump mated
with a three-stage high vacuum oil diffusion pump. This part of the
pumping system was connected to the reservoir with a large diameter

TABLE I

DIMENSIONAL SPECIFICATIONS OF RAREFIED VISCOSEAL NO. 1

Parameter	Value
Housing diameter	$= 2.0088 \pm 0.0003$ in.
Shaft diameter, D	$= 2.0005 \pm 0.0001$ in. (cold)
Radial mean clearance, $\bar{c}$	$= 0.00418 \pm 0.0002$ in. (cold)
Seal axial length, L	$= 4.530 \pm 0.005$ in.
Number of groove starts, N_S	$= 16$
Groove axial width, b	$= 0.03111 \pm 0.0003$ in.
Land axial width, a	$= 0.03235 \pm 0.0003$ in.
Groove depth, h	$= 0.03065 \pm 0.0003$ in.
Groove helix angle	$= 9.30°$
$\gamma = b/(a + b)$	$= 0.4902$
$\beta = (h + c)/c$	$= 8.333$ (cold)
Aspect ratio, $b \cos \alpha/h$	$= 1.0017$
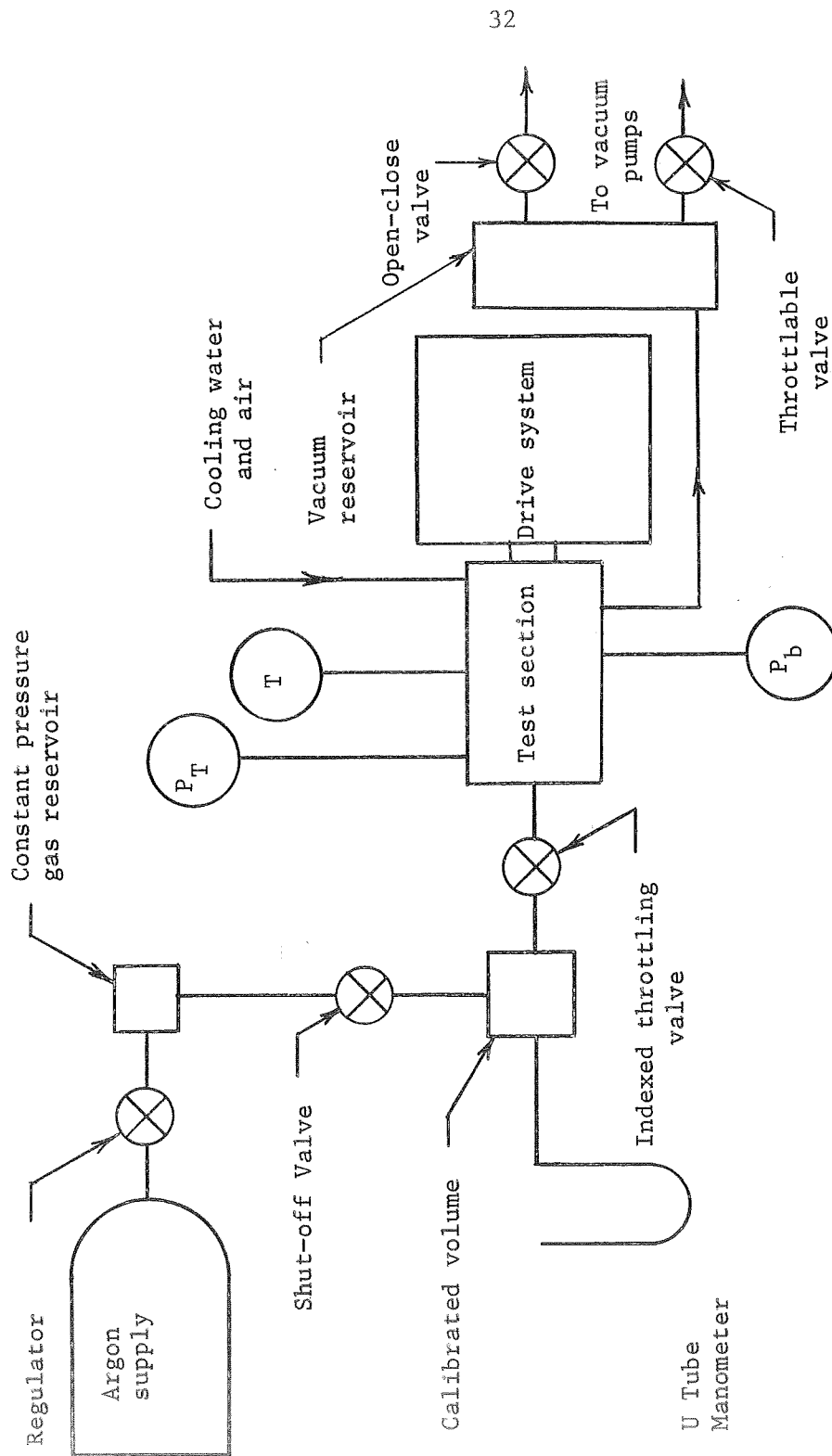
Figure 4. Schematic Diagram of the Experimental Test Apparatus.

open-or-close vacuum valve. The second pumping system was composed of another single stage rotary oil-sealed mechanical pump mated with a positive displacement roots blower type vacuum pump. This portion of the pumping system was connected to the reservoir through a throttlable high vacuum valve. Through manipulation of the two connecting valves it was possible to regulate the pumping speed over a suitable range of downstream test section pressures. The complete vacuum pumping system was capable of attaining pressures to 10^{-5} millimeters of mercury with a blanked-off system.

Instrumentation

The radial alignment of the shaft within the housing was determined by the use of five proximity detectors manufactured by the Bentley-Nevada Corporation. These probes were located near either end of the viscoseal section. When viewed from the shaft drive end of the test section, the probes of the first set were located at 12, 3, and 6 o'clock positions, and the probes of the second set were located at 12 and 3 o'clock positions. The arrangement of the probes permitted the shaft to be aligned within the housing to a value of eccentricity ratio(shaft centerline deviation/mean radial clearance) on the order of 0.05. The probes were also used to obtain dynamic measurements of the thermal growth of the shaft caused by the graphite ring seal friction when the shaft was rotating. The output gains of the detector amplifiers were individually adjusted and calibrated to ensure a linear output voltage of the probes versus the clearance gap over the necessary range.

Pressure measurements upstream and downstream of the viscoseal were obtained using both McLeod gauges and an absolute aneroid type gauge. The McLeod gauge is normally considered to be a primary standard [26], but after previous attempts [27] to use thermocouple gauges and cold cathode gauges, it was apparent that McLeod gauges were the only instruments capable of giving the desired accuracy and reproducibility. The McLeod gauges utilized were the GM-100A gauge manufactured by the Consolidated Vacuum Corporation and are described in detail in Reference [27].

Temperature measurements of the argon entering the high pressure end of the viscoseal test section were made early in the experimental program using a thermocouple. A comparison of the measured gas temperature with the ambient (room) temperature revealed that the error involved in using room temperature instead of the actual gas temperature was less than one percent. Therefore the gas temperature was taken to be 297°K in all data calculations.

Speed measurements of the viscoseal shaft were made using a magnetic pickup located near the attachment nut for the drive belt pulley on the high speed spindle. The pulses from the pickup were registered using an electronic counter to obtain shaft rpm. The speed measurements were independently verified using a calibrated hand held tachometer in the low rpm range and a calibrated strobotac over the entire speed range of 0 to 35,000 rpm.

The molecular flow rate through the viscoseal test section was determined using a variation of a constant pressure method developed by J. R. Downing [26] for the measurement of pumping speeds of vacuum

pumps. The technique consists of application of the perfect gas equation

of state to known gas volumes at two different time periods. In brief,

the flow measurement is obtained by adjusting the indexed valve of

Figure 4, page 32, to a desired setting and waiting for steady state to

be achieved in the test section as indicated by pressure and proximity

probe measurements. The shut-off valve leading from the constant

pressure gas reservoir is then closed and the rate of rise of manometer

fluid in the right hand side of the manometer is observed. With knowledge

of the manometer cross sectional area, the rate of fluid rise, the value

of the calibrated volume, the initial and final pressures in the

calibrated volume, and the gas temperature, the molecular flow rate is

calculated in the following manner:

Consider the flow measurement diagram of Figure 5. Let

V_o = calibrated volume including tank and manometer down to

the zero deflection line, "0"

P_o = atmospheric pressure

H_1 = initial manometer deflection

H_2 = final manometer deflection

A_m = cross section area of manometer tube

W = specific weight of manometer fluid

From fluid statics:

$$P_1 = P_o + 2WH_1$$

$$P_2 = P_o - 2WH_2.$$

The corresponding volumes are:

$$V_1 = V_o + H_1 A_m$$

$$V_2 = V_o - H_2 A_m.$$
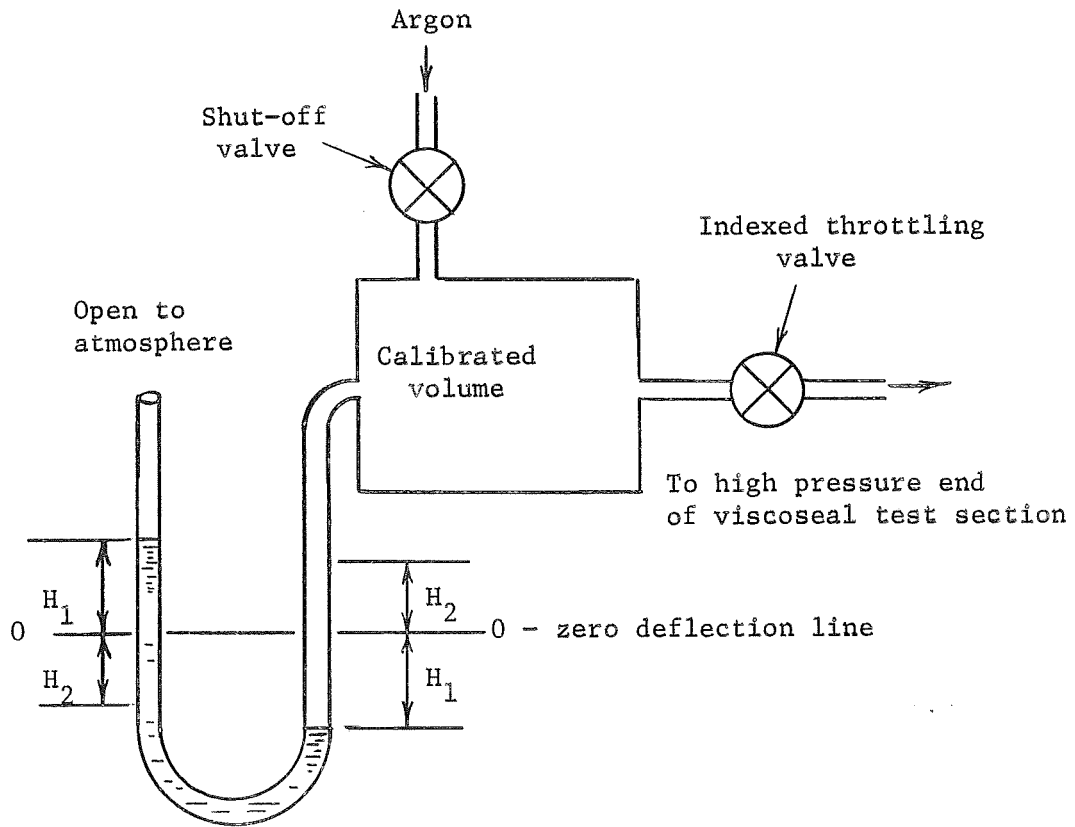
Figure 5. Flow Measurement Schematic Diagram.

Applying the perfect gas equation of state,

$$PV = NKT, \tag{3-1}$$

on a molecular basis to determine the number of molecules within the
system at time (1) and time (2), then,

$$\Delta N = N_1 - N_2 = \frac{P_1 V_1}{KT_1} - \frac{P_2 V_2}{KT_2} . \tag{3-2}$$

Assuming isothermal conditions and substituting for the pressures and
volumes, Equation (3-2) simplifies to,

$$\Delta N = \frac{H_1 + H_2}{KT} \{A_m[P_o + 2W(H_1 - H_2)] + 2WV_o\} . \tag{3-3}$$

The flow measurement system was operated experimentally such that

$$H_1 = H_2.$$

Letting

$$H = H_1 + H_2$$

and Δt be the time period for the total deflection H, then the molecular
flow rate is

$$\overset{\circ}{N} = \frac{\Delta N}{\Delta t} = \frac{H}{\Delta t KT} \{A_m P_o + 2WV_o\}. \tag{3-4}$$

In the experimental fabrication of the flow measurement system,
a small, inches of water range, differential pressure gauge was unfortunately
connected to the system within the elements of the calibrated volume.
It was initially felt that the change in volume of the gauge bellows
with changes in pressure was negligible in comparison to that of the
manometer fluid, and all experimental data were obtained in this
configuration. Subsequent investigations revealed that it was necessary
to account for the change in volume of the pressure gauge as a function

of the measurement system pressure. Letting f(H) equal the volume

change of the pressure gauge as a function of the manometer head travel

H, then Equation (3-4) is correctly written as

$$\dot{N} = \frac{\Delta N}{\Delta t} = \frac{1}{\Delta t KT} \{H[A_m P_o + 2WV_o] + 2P_o f(H)\} . \tag{3-5}$$

The volume relationship between the pressure gauge expansion and

contraction was carefully measured experimentally to determine f(H).

The following values were determined for the constants of

Equation (3-5):

$A_m = 0.0250 \ cm^2 \pm 5\%$

$V_o = 114.75 \ cm^3 \pm 5.0\%$

$W = 796 \ dynes/cm^3 \pm 1\%.$

The basic premise for the measurement system rests in the fact that

while the pressure in the calibrated volume does change slightly, less

than $\pm 1\%$, it still remains very close to atmospheric pressure. Thus,

the change in flow rate through the valve is negligibly affected by

the slight decrease in the pressure within the calibrated volume during

the course of a measurement.

Experimental Procedure

Experimental data of two different types were obtained for the

operation of the viscoseal in the rarefied regime. These may be described

as net flow leakage data and sealing coefficient data. The operational

procedure utilized in gathering the data differed only in respect to

shutting off the argon gas supply when obtaining sealing coefficient data.

All data were acquired by the coordinated adjustment of the gas supply rate, the vacuum pumping speed, and the seal shaft drive speed followed by a time stabilization period. Following achievement of steady state, final readings of the gas flow rate, pressures upstream and downstream of the viscoseal, and the proximity probes were made. The proximity probes were used to record the seal clearance which decreases slightly with increasing shaft speed due to the friction of the graphite ring vacuum seal.

Data Utilization

The viscoseal performance data for both the net flow leakage tests and the sealing coefficient tests were correlated versus an index of the flow rarefication, Knudsen number. As explained in Chapter II, the mean radial clearance, $\bar{c}$, was selected as the viscoseal characteristic dimension. Thus using the Chapman relationship for the mean free path, the experimental values for Knudsen number were determined using Equation (2-41) which is repeated here for clarity,

$$N_K = \frac{\lambda}{\bar{c}} = \frac{\mu (2\pi \frac{R_o}{M} T)^{1/2}}{2\bar{P}\ \bar{C}} \,.$$

The mean free path was based on the average seal section pressure

$$\bar{P} = \frac{P_T + P_b}{2} \,. \qquad\qquad (3\text{-}6)$$

The molecular flow rates for the net flow leakage data were calculated using Equation (3-5). These data were revised to specific molecular flow rates by dividing by the pressure drop, ΔP, across the viscoseal, or

$$\frac{\dot{N}}{\Delta P} = \frac{H[A_m P_o + 2WV_o] + 2P_o \; f(H)}{(P_T - P_b)\Delta t KT} \; . \qquad (3\text{-}7)$$

The sealing coefficient data were calculated from the zero net leakage tests using

$$\Lambda = \frac{6\mu UL}{\Delta P \bar{c}^2} = \frac{6\mu UL}{(P_T - P_b)\bar{c}^2} \; . \qquad (3\text{-}8)$$

Investigations Conducted

As previously stated, two types of different but related data were obtained. These were sealing coefficient performance data where there was no net mass transport across the viscoseal and net leakage performance data where leakage flow does occur. Net leakage data were obtained over the maximum possible range of rarefication for shaft speeds of zero, 5,000, 10,000, and 30,000 rpm. Corresponding rarefied sealing coefficient data were also obtained over the maximum range of rarefication at these same shaft speeds. These data are presented and discussed in Chapter IV and are tabulated in Appendix E.

In addition to the rarefied investigations, a supporting continuum sealing coefficient investigation was conducted at atmospheric conditions using air as the sealant fluid. This continuum investigation is summarized in Appendix C.

Experimental Uncertainty

A detailed analysis was performed to estimate the propagated uncertainty in the final performance parameters based on the individual

uncertainties of all measured variables. The analysis was performed using standard statistical techniques after postulating a normal distribution in the uncertainty of each variable. This method of analysis assumes all errors are random in nature. Considerable effort was expended to minimize any error of a systematic nature.

The propagated uncertainties, in general, are not constant and vary with the degree of rarefication. The uncertainty in the specific molecular flow rate, $\mathring{N}/\Delta P$, of Equation (3-7) is $\pm$ 5.1 percent at an Inverse Knudsen Number of 27 where the calibrated volume, V_o, contribution is 84 percent of the total. The uncertainty in the specific molecular flow rate increases to $\pm$ 8.9 percent at an Inverse Knudsen Number of 0.50 where the uncertainty in the differential pressure, ΔP, contributes 72 percent of the total. The ability to determine the Inverse Knudsen Number of Equation (2-41) is estimated at $\pm$ 4.8 percent for $1/N_K$ equal to 27 and increases to $\pm$ 5.7 percent for $1/N_K$ equal to 0.50. The propagated uncertainty estimate in the sealing coefficient, Λ, of Equation (3-8) is insensitive to the degree of rarefication and remains at essentially $\pm$ 9.6 percent. The uncertainty in the radial clearance, c, contributes approximately 99 percent of the propagated uncertainty estimate for Λ. It should be noted that the clearance uncertainty is controlled by the ability to establish the diameters of the seal shaft and housing and not by any limitations of the proximity probe system.

The uncertainty of the clearance Reynolds number of Equation (C-1) in Appendix C has been estimated at $\pm$ 4.9 percent where the radial clearance contributes approximately 94 percent of the total.

All uncertainties are stated to a confidence level of 95 percent.

CHAPTER IV

RESULTS AND CONCLUSIONS

As stated in Chapter I, this study of the rarefied-gas viscoseal
was initiated to expand the basic understanding of its operation under
low density conditions. A combined analytical and experimental investi-
gation was selected as the approach to the problem solution. The relation-
ship between these two phases of the research program and the results and
and conclusions of this study are discussed in this Chapter.

Net Leakage Investigation

A net leakage flow condition from the high pressure end to the low
pressure end exists in the viscoseal when the viscous pumping action is
insufficient to overcome the pressure induced and diffusive flows in the
grooves and through the annular clearance space. The experimental
data for these experiments are shown in Figure 6 for shaft speeds of
zero, 5,000, 10,000, and 30,000 rpm. These data are presented as the
specific leakage rate in molecules per second and micron of pressure
difference across the seal versus Inverse Knudsen Number. Theoretical
curves are shown to permit comparisons of the experiments and theories.
In general, the developed theoretical models predict the trends of the
experimental data; however, some deviations between the theories and
experiments exist in certain regions.

Figure 6. Net Leakage Flow Versus Inverse Knudsen Number, Seal No. 1

One test for any theoretical viscoseal model is its ability to predict the leakage flow for the non-rotational shaft condition. In this case the speed sensitive terms of Equations (2-42) and (2-44) go to zero and only the pressure induced terms remain. For the static case it is obvious that the experimental data falls below the theoretical curves for continuum values of Inverse Knudsen Number approaching 100. In this regime no differences between the theoretical equations exist, and these data are really a test of the continuum model of Boon and Tal since rarefied effects are negligible. In the basic Boon and Tal model it will be recalled that boundary conditions are applied to the moving top wall and to the bottom of the groove but not to the groove side walls. Depending on the relation of the groove width to its depth (groove aspect ratio), this omission may or may not be of significance. When the groove is very wide in comparison to its depth, one would expect the omission of the boundary condition on the side walls to be of minor importance. As the aspect ratio decreases and approaches unity, however, the effects of the side walls become of the same order of magnitude as the top and bottom walls of the groove and should be considered. The aspect ratio of the experimental geometry is essentially unity and the difference between the theory and the experimental data in the continuum regime is largely attributed to the omission of the side wall boundary conditions.

As the flow becomes more rarefied, as indicated by the decrease in Inverse Knudsen Number, the agreement between the theory and the experimental data is improved although the theoretical predictions remain high. The influence of the groove side walls would be expected to be of

a greater magnitude under continuum conditions as opposed to rarefied

conditions. Under continuum flow the fluid adjacent to the walls has a

relative velocity to the wall of zero while under rarefied conditions the

fluid velocity in the vicinity of the walls is finite being the "slip

velocity."

Figure 6, page 44, shows the theoretical solutions for the static

rpm case. The solid line solution, Equation (2-42), indicates the flow

obtained by application of the slip boundary conditions to the Reynolds

equations. The second solution, Equation (2-50), indicated by the dashed

line, is the composite solution obtained by correcting the slip-modified

Reynolds equations for the number of molecules which collide with the

walls and consequently cannot experience slip boundary conditions,

Equation (2-44), and then adding the self-diffusion flows both in the

grooves and the annular space. It may be observed that there is

essentially no difference in the two solutions until the Inverse Knudsen

Number decreases below a value of approximately 3.0. Although the

difference in these two static solutions increases with increased

rarefication the composite solution is only 15 percent higher than the

solution of Equation (2-42) at an Inverse Knudsen Number of 0.10. Table

II presents a comparison of the two solutions and permits an examination

of the contributions to the composite solution. Examination of the

table shows that the diffusion flow contributions in both the annular

space and the sixteen grooves are only one percent of the total composite

flow at an Inverse Knudsen Number of 7.0 and decrease rapidly with

decreased rarefication. At an Inverse Knudsen Number of 0.01 it can be

observed that the diffusion contributes 92 percent of the total composite

TABLE II

NET LEAKAGE SOLUTIONS X 10^{-14} FOR SEAL NO. 1 AT ZERO RPM

$1/N_K$	$\mathring{N}/\Delta P$ Cont. + slip No. Part. Corr. Eq. (2-42)	$\mathring{N}/\Delta P$ Composite Solution - Eq. (2-50)			
		Cont. + slip Part. Corr. Eq. (2-44)	Annulus Diffusion Eq. (2-47)	Groove Diffusion Eq. (2-49)	Composite Flow Eq. (2-50)
1×10^{-2}	2.22	0.198	1.92	0.48	2.60
3×10^{-2}	2.24	0.514	1.69	0.42	2.62
7×10^{-2}	2.30	0.951	1.41	0.34	2.70
1×10^{-1}	2.33	1.18	1.30	0.30	2.78
3×10^{-1}	2.58	1.99	0.87	0.17	3.03
7×10^{-1}	3.08	2.78	0.57	0.086	3.44
1×10^{0}	3.45	3.23	0.45	0.053	3.73
3×10^{0}	5.92	5.84	0.19	0.022	6.05
7×10^{0}	10.8	10.8	0.090	0.0096	10.9
1×10^{1}	14.5	14.5	0.064	0.0068	14.6
3×10^{1}	39.2	39.2	0.022	0.0023	39.2
7×10^{1}	88.4	88.4	0.0094	0.0010	88.4
1×10^{2}	125.0	125.0	0.0065	0.0007	125.0

solution and the flow is essentially free molecular. The moderately close

agreement between the rather complex composite solution of Equation (2-50)

and the more simple solution of Equation (2-42) over the entire range of

rarefication for the viscoseal is comparable to that obtained similarly

for flow through both long tubes and annuli.

Net leakage data for the three dynamic operating speeds of 5,000,

10,000, and 30,000 rpm are also shown in Figure 6, page 44. A single set

of theoretical curves is shown for these data since there is negligible

difference between the two solutions previously discussed in this rare-

fication regime. Table III presents a flow comparison tabulation for the

5,000 rpm solutions since this speed has the most rarefied conditions of

the three. The difference between the 5,000 rpm dynamic solutions cannot

be distinguished on Figure 6. Examination of the values of Table III shows

that the difference in the two solutions is approximately one percent at an

Inverse Knudsen Number of 10.0. While the trends of the theoretical

solutions of Equation (2-42) for the dynamic cases do match the experimental

data, considerable differences between theory and data do exist. Based

on the degree of agreement that existed between theory and experiment

for the zero rpm case, the data for the dynamic tests indicate that the

flow predictions of the rotor induced terms of Equation (2-42) and Equation

(2-44) are in excess of the actual rotor induced pumping obtained.

The specific molecular flow rate equations for the dynamic speeds are

pressure ratio sensitive as may be noted by examining Equations (2-42)

and (2-44). The theoretical curves presented have been matched to the

measured experimental pressure ratios.

TABLE III

NET LEAKAGE SOLUTIONS X 10^{-14} FOR SEAL NO. 1 AT 5,000 RPM

$1/N_K$	$\dot{N}/\Delta P$ Cont. + slip No. Part. Corr. Eq. (2-42)	$\dot{N}/\Delta P$ Composite Solution - Eq. (2-50)			
		Cont. + slip Part. Corr. Eq. (2-44)	Annulus Diffusion Eq. (2-47)	Groove Diffusion Eq. (2-49)	Composite Flow Eq. (2-50)
7.0	0.161	0.132	0.075	0.0089	0.216
8.0	1.40	1.38	0.067	0.0078	1.450
10.0	3.90	3.88	0.054	0.0063	3.940

The propagated experimental uncertainties in $\dot{N}/\Delta P$ and $1/N_K$ discussed

in Chapter III are sufficiently small to preclude their display on Figure

6, page 44, their being of the order of the data symbols.

Sealing Coefficient Investigation

Performance of a viscoseal at the particular condition for which

there is no net mass transport across the seal represents a very special

operating condition but one of particular interest to many investigators.

Vreeburg [1], Baron [4], King [6], Hodgson and Milligan [7], Boon and Tal [15],

and Stair [16, 17] have all included analyses and/or experimental

investigations of viscoseal operation at this condition. In Chapter II

after developing the slip-modified Reynold's solution given by

Equation (2-28), the flow was set equal to zero and the sealing coefficient

parameter

$$\Lambda = \frac{6\mu UL}{\Delta P C^2}$$

evaluated as shown in Equation (2-29). Sealing coefficient data were

obtained over the maximum possible range of rarefication for shaft speeds of

5,000, 10,000, and 30,000 rpm and are shown on Figure 7 together with

corresponding theoretical curves of Equation (2-29). The agreement between

theory and experiment is fair; however, significant deviations do exist.

The theory does predict the correct trend of the sealing degradation as

conditions become more rarefied, however, the theory is optimistic in

predicting lower than measured values of sealing coefficients. It may be

observed that the experimental data indicate that the sealing coefficient

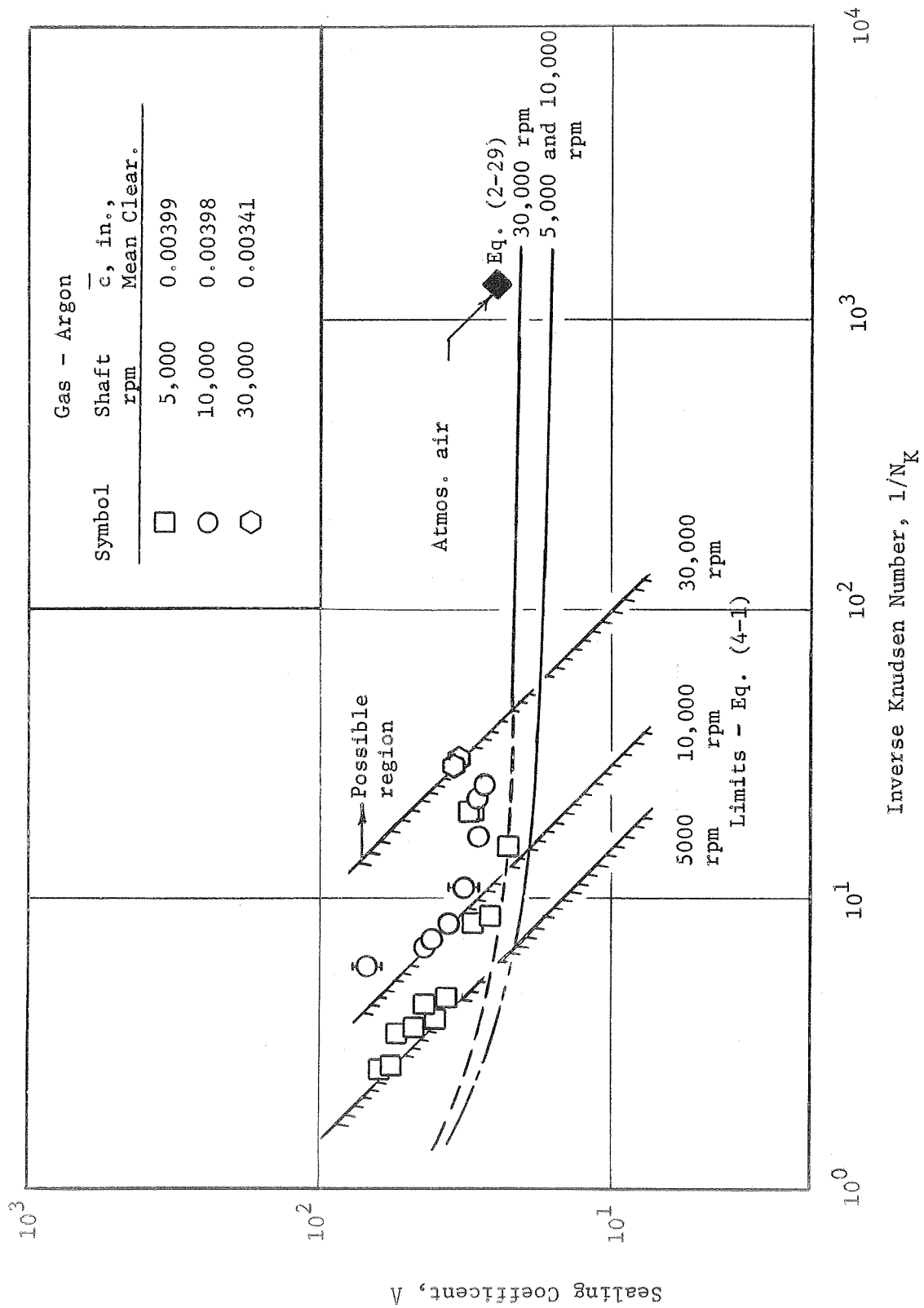parameter becomes speed sensitive as the sealant gas becomes rarefied,

Figure 7. Sealing Coefficient Versus Inverse Knudsen Number, Seal No. 1.

and this speed dependence is not predicted by the developed theory of
Equation (2-29). The sensitivity to shaft speed for the rarefied-gas
viscoseal is also unique from that of operation in the laminar continuum
regime where the sealing coefficient is independent of shaft speed [7, 18].
This continuum characteristic may be seen by noting the asymptotic behavior
of the experimental data of 5,000 and 10,000 rpm as the continuum regime
is approached ($1/N_K > 100$). These data may be compared since the mean radial
clearance is essentially the same for both speeds. A separate theoretical
curve is shown for the 30,000 rpm data due to the difference in the mean
radial clearance.

Figure 7 also shows the average sealing coefficient value for the
viscoseal operating at laminar continuum conditions using atmospheric air
as the sealant fluid. This continuum data agrees well with the rarefied
data extrapolated to this regime. As pointed out in Chapter II, the
rarefied-gas sealing coefficient theories of Equations (2-29) and (2-38)
reduce to the basic Boon and Tal theory of Equation (2-30) as the continuum
regime is approached. Again the theoretical predictions are optimistic
in comparison to the measured data. Appendix C contains a more detailed
account of the laminar continuum investigations.

Examination of the theoretical solution of Equation (2-29) reveals
that under very rarefied conditions the model can predict a seal pressure
differential, ΔP, which may exceed the magnitude of the upstream or fore
pump pressure. This solution would imply a negative absolute value for the
downstream pressure, a condition which cannot occur in reality. A limiting
criteria to be applied to the theoretical solutions to avoid this condition
is predictable by considering the variables involved. Figure 7 presents the

sealing coefficient, Λ, versus the Inverse Knudsen Number, $1/N_K$. As

stated in Chapter III, Knudsen number

$$N_K \equiv \frac{\lambda}{c} = \frac{\frac{\mu(2\pi\frac{R_o}{M}T)^{1/2}}{}}{2\overline{P}c}$$

is based on the average pressure in the seal

$$\overline{P} = \frac{P_T + P_b}{2} = \frac{2P_T - \Delta P}{2} \, .$$

As the downstream pressure approaches zero, then ΔP approaches the

upstream pressure and for this limiting condition

$$\overline{P} \sim \frac{\Delta P}{2} \, .$$

Thus, the Inverse Knudsen Number variable may be written as

$$(1/N_K) = \frac{\Delta Pc}{\mu(2\pi\frac{R_o}{M}T)^{1/2}} \, .$$

The Sealing Coefficient variable is defined as

$$\Lambda = \frac{6\mu UL}{\Delta Pc^2} \, .$$

Solving for ΔP in the Inverse Knudsen Number relationship and

substituting this into the above equation gives the limiting functional

relationship

$$\Lambda_{limit} = \{\frac{6UL}{c(2\pi\frac{R_o}{M}t)^{1/2}}\} \frac{1}{(1/N_K)} \, . \tag{4-1}$$

For a given seal geometry, gas, temperature, and operating speed, the

limiting seal coefficient function varies inversely with the Inverse

Knudsen Number, $1/N_K$. On a logarithmic plot such as Figure 7, this relation

will plot as a straight line with a slope of minus unity. Points which
fall above and to the right of this line are possible while those which
fall below and to the left are not possible in that a negative absolute
pressure downstream is implied. The limiting relation of Equation (4-1)
is speed sensitive and thus the limit condition can be established for each
selected shaft speed. Limit curves for speeds of 5,000, 10,000, and 30,000
rpm from Equation (4-1) are shown on Figure 7, page 51. The experimental
sealing coefficient data agree well with these limit curves and all points
fall within the "possible"regions. In addition, the speed sensitivity of
the experimental data agrees with that indicated by Equation (4-1). It
should be noted that the limiting function of Equation (4-1) results from
a limit condition of the variables involved and applies to any and all
viscoseal analyses using these variables.

In view of the limiting functional relationship just established,
the theoretical curves of Equation (2-29) on Figure 7 are dash-lined
pass the applicable limit curve for a particular speed to show the
solution trends and trends only. Theoretical sealing coefficient
predictions are not presented for the composite flow solution. There is
negligible difference between the composite sealing coefficient solution
and that predicted by Equation (2-29) at the degree of rarefication that
exists for the sealing coefficient data. This is in agreement with the
observation of Table III for the net leakage solution for 5,000 rpm.

The propagated uncertain in Λ is typically shown on Figure 7 by the
vertical bars on selected data points. The uncertainty in $1/N_K$ is of
the order of the data symbol width.

The relationship which exists between the net leakage flow of Figure 6, page 44, and the sealing coefficient data of Figure 7, page 51, can best be shown by reference to Figure 8. Here is shown the family of net leakage curves that exist as functions of the seal pressure ratio for a fixed shaft speed as predicted by Equation (2-42). The curves progress to the left for increasing values of pressure ratio until the $(r_p + 1)/(r_p - 1)$ factor in the speed sensitive term of the equation approaches unity. When the family of net leakage flow curves are extended to the zero net flow condition via the broken graph, a corresponding sealing coefficient condition may be indicated for each of these pressure ratio curves. Operating the rarefied viscoseal at "negative" conditions of net leakage flow is simply another way of saying the viscoseal has now become a positive flow pump.

Comparisons with Data of Other Investigators

As pointed out in Chapter I, relatively few experimental investigations of rarefied-gas viscoseal performance have been conducted. Experimental data obtained by other investigators are presented in the three following figures. Also presented in these figures are the results obtained by the theoretical model, Equation (2-29), which has been developed. The experimental data of these other investigators are in sealing coefficient or equivalent form, and as previously stated, there are essentially no differences between the theoretical predictions of Equation (2-29) and (2-50) over the pertinent rarefication range.
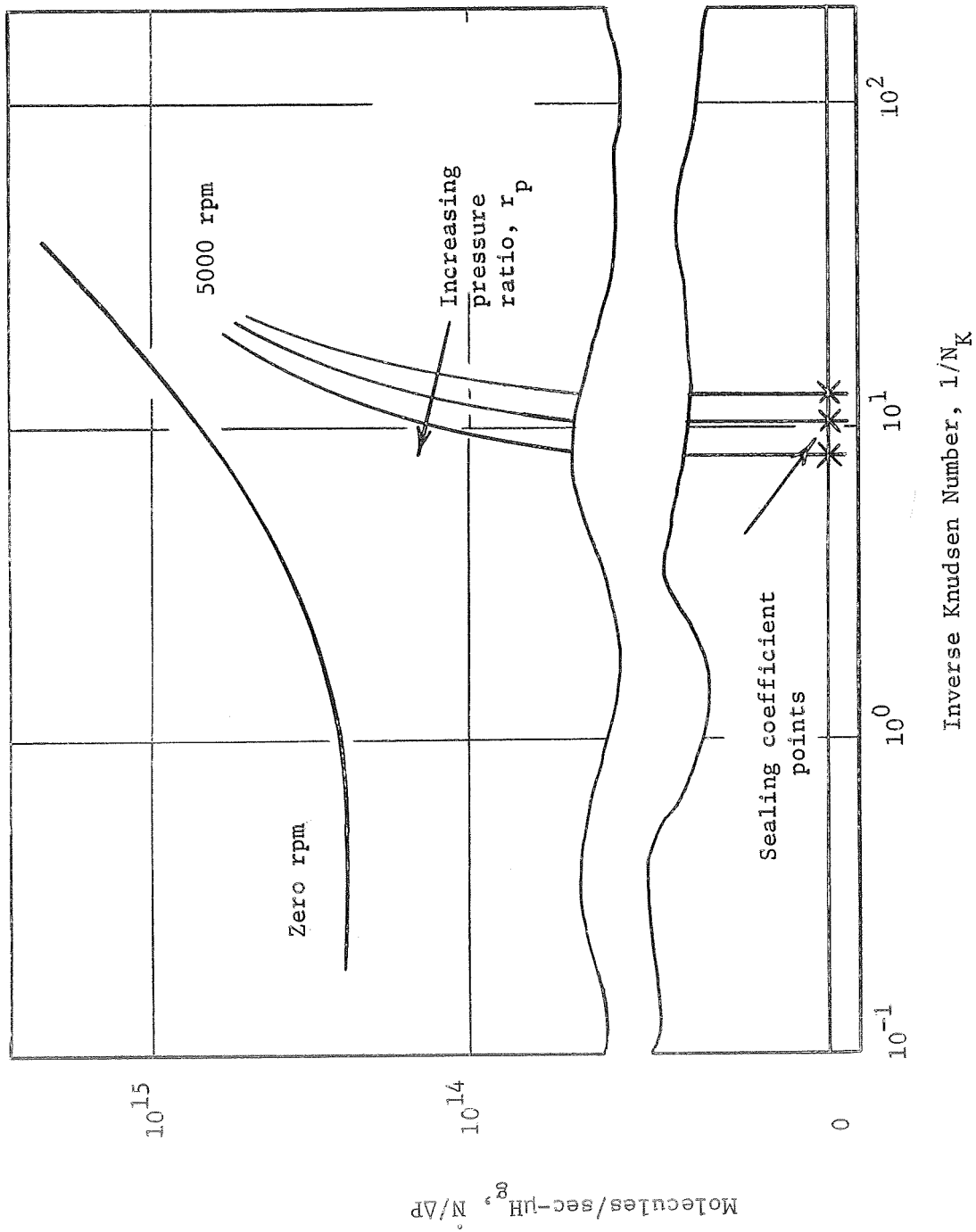
Figure 8. Relation Between the Net Leakage Flow and the Sealing Coefficients

Figure 9 presents the data of Hodgson and Milligan [7] using
atmospheric air as the sealant fluid. These data are in the continuum
regime at an average Knudsen number of $\overline{N}_K = 0.00147$. The experimental
results indicate a slightly poorer sealing coefficient value than that
predicted by the theory but agree within the tolerances in sealing
coefficient which result from the geometric uncertainties associated
with the seal dimensions [7]. The degradation in seal performance as
the density becomes lower is indicated by the theoretical curves.

In Figure 10 the data of Baron [4], also for air, are compared with
the theoretical predictions from Equation (2-29). Baron's sealing
parameter is related to the sealing coefficient in the manner shown on
the ordinate. The data of Baron, while more rarefied, $\overline{N}_K = 0.014$,
than that of Hodgson and Milligan, are still within the continuum regime.
The theory certainly predicts the trends of the data although there is a
significant deviation between theory and experiment. Again the theory
is optimistic in its prediction of the viscoseal performance.

In Figure 11 the data of King [6] for air are compared with
theoretical predictions. Some of these data are in the non-continuum
regime. As shown in the figure, the theory indicates that non-continuum
effects will occur for Knudsen Numbers greater than 0.01 in the form of a
decrease in sealing performance. The data also indicate this same trend
although there is a significant deviation between theory and experiment.
The limiting function of Equation (4-1) is also shown for a shaft speed of
14,000 rpm and raises a question concerning the validity of one of King's
data points. Similar to the other comparisons, the theory is optimistic
in its prediction of seal performance.
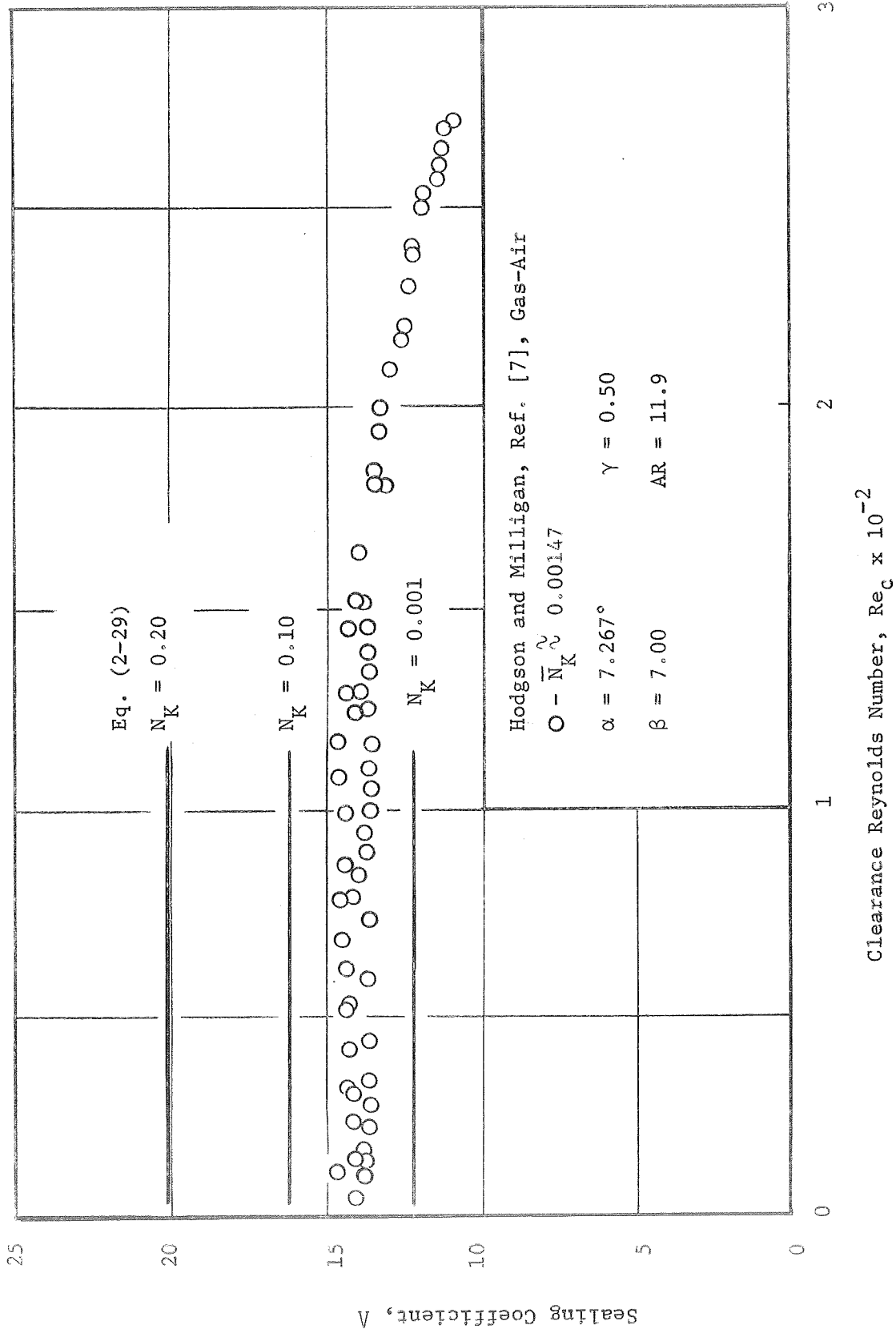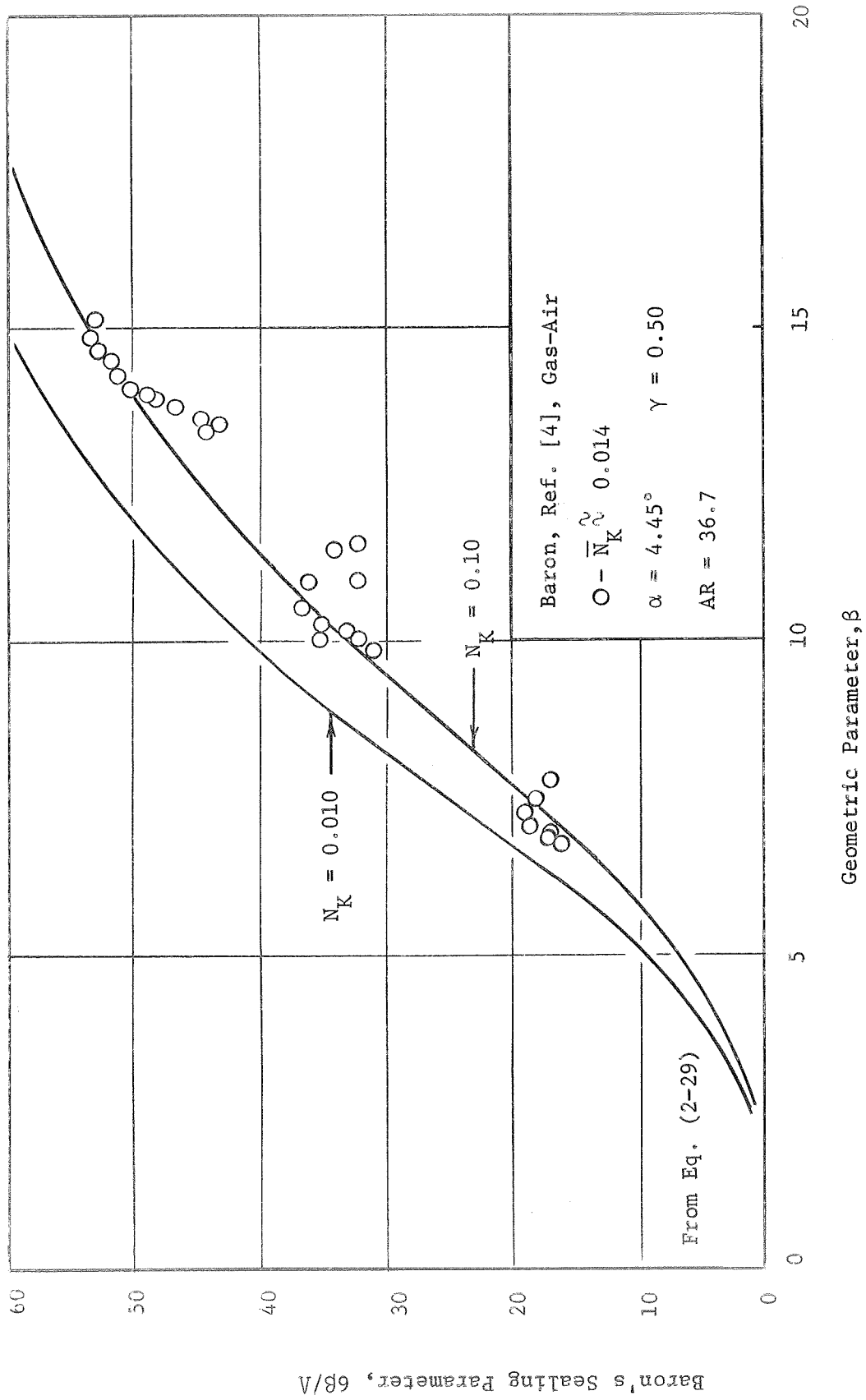
Figure 9. Sealing Coefficient Versus Clearance Reynolds Number – Hodgson and Milligan.

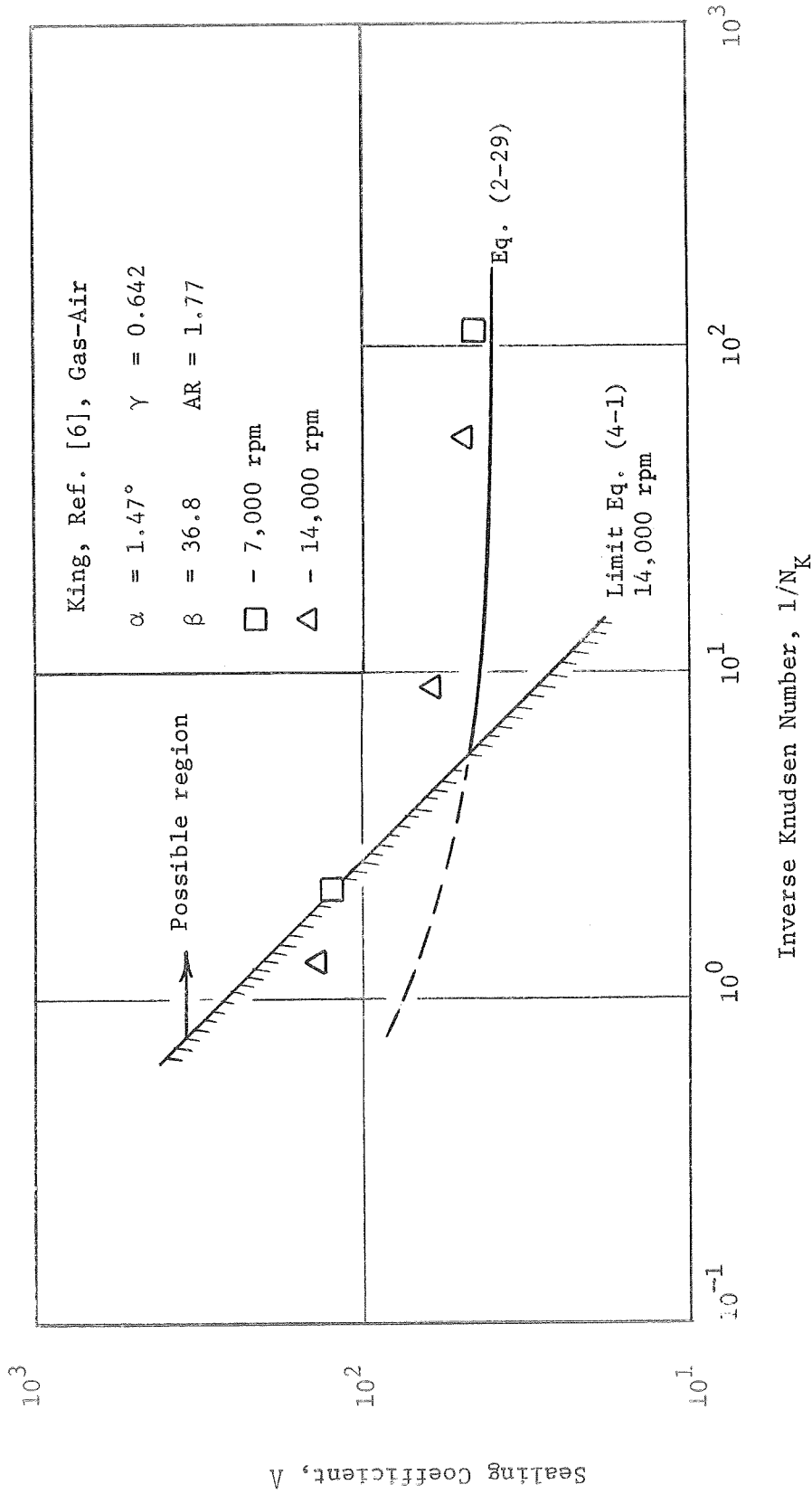Figure 10. Baron's Sealing Parameter Versus Seal Geometric Parameter, β.

Figure 11.   Sealing Coefficient Versus Inverse Knudsen Number – King.

Final Conclusions

At the close of this study it is desirable to enumerate some of the major conclusions of the investigation conducted. While a number of these have been discussed in the preceding material, where applicable, it is profitable that these be reviewed and generalized comments presented.

The developed theoretical models predict the trends for both the net leakage and the sealing coefficient data, however deviations of sufficient magnitude exists to prevent their indiscriminate use. A major source of the difficulties with the theory is the basic limitations of the laminar continuum model of Boon and Tal which was selected as the beginning point for the rarefied analysis. The continuum data of Figure 6, page 44, show rather conclusively that the model of Boon and Tal does not adequately predict the flow when dealing with grooves having the width of the same order of magnitude as the depth. While it is realized that the viscoseal groove geometries utilized for purely continuum sealing are usually very shallow, to the author's knowledge, the need for restricting the model usage to grooves of high aspect ratio has not been emphasized. It is anticipated that the developed rarefied models will more closely predict the seal performance as the aspect ratio becomes larger although data are not presently available to substantiate this. A theoretical laminar continuum model which includes the groove side wall boundary condition is needed and is presently being pursued by Patterson [8]. With this improvement, the use of slip boundary conditions coupled with the correction for particles which do not experience slip plus the addition of the self-diffusion flows in the grooves and the annular space still appears to be

the most fundamental approach for obtaining a theoretical rarefied solution. It should be borne in mind, however, that while this is the more rigorous approach, the tremendous increase in complexity and time of obtaining this composite solution appears to buy only slight improvements in the theoretical model based on the information at hand. From the viscoseal designer viewpoint, the use of the relatively simple rarefied model obtained by application of slip boundary conditions to a proper continuum model does provide an acceptable method of including moderately rarefied effects. When this is coupled with the limiting function for the sealing coefficient parameter, this does provide a practical design tool for establishing an upper limit for rarefied-gas viscoseal performance.

This study has amply illustrated the real need for more detailed experimental performance data on rarefied-gas viscoseals to provide a test of the developed theoretical models. These experimental programs need to include not only sealing coefficient measurements but also net leakage investigations as these tests can provide real insight into the model. Tests of sealing coefficient do not provide the detailed visibility into the model that is afforded with the net leakage type of experiments. The sealing coefficient parameter, while of considerable interest, does constitute a very special operating condition for the viscoseal and one that is not often realized in application.

As previously stated, this investigation was a portion of "A Fundamental Study in Low-Density Gas Dynamics," supported at the University of Tennessee by the National Aeronautics and Space Administration. Continued investigations of rarefied-gas viscoseals, both experimentally and analytically, are in progress.

BIBLIOGRAPHY

BIBLIOGRAPHY

1. Vreeburg, Jan. P. G., "Investigations of Laminar Flow Patterns and Pressure Generation in a Viscoseal Geometry." Doctoral Dissertation, The University of Tennessee, Knoxville, Tennessee, March 1969.

2. Fisher, Charles F., Jr., "An Investigation of Interface Stability and Its Relation to Gas Ingestion in Viscoseals." Doctoral Dissertation, The University of Tennessee, Knoxville, Tennessee, August 1969.

3. Stair, W. K., "The Viscoseal, A Survey." Report ME-5-62-2, The University of Tennessee, Knoxville, Tennessee, May 1962.

4. Baron, H. W., "Experimenten aan een hydrodynamisch werkende spiraalgroef-asafdichting," De Ingenieur, Vol. 74, No. 32, 1962, pp. 144-150.

5. Hodgson, J. N., "SNAP-8 Seals-to-Space Development Test Program Volume II - Molecular Pump," NASA-CR-54234, May 1964.

6. King, A. E., "Screw Type Shaft Seals for Potassium Lubricated Generators," Supplement to IEEE Transactions on Aerospace, June 1965, pp. 471-479.

7. Hodgson, J. W. and M. W. Milligan, "Visco-Type Gas Sealing." Presented at the Fourth International Conference on Fluid Sealing. ASLE Preprint FICFS Number 34, May, 1969.

8. Patterson, K. E., "An Analytical Model for the Prediction of Viscoseal Performance in the Regime from Continuum to Free-Molecule Flow." Master's Thesis, The University of Tennessee, Knoxville, Tennessee, (to be released approximately August 1970).

9. Weber, S., "Uber Deu Zusammenhang Zwischen Der Laminaren Stromund Der Reineu Gase Durch Rohre Und Dem Selbsdiffusions-Koeffizienten." Math-Fysiske Meddelser, Band 28, No. 2, 1954. Translation, "The Connection Between the Laminar Flow of Pure Gases Through Tubes and the Self-Diffusion Coefficient." Translated by R. Ash and J. B. Sykes, Atomic Energy Research Establishment Trans. 946, April 1963.

10. Milligan, M. W., "Low-Density Gas Flow in Long Tubes." American Institute of Aeronautics and Astronautics Journal, Vol. 4, No. 4, April 1966, pp. 745-746.

11. Milligan, M. W., "Fundamental Study in Low-Density Gas Dynamics." Mechanical and Aerospace Engineering Research Report AE-66-023-1, University of Tennessee, November 1966.

12. Milligan, M. W., P. W. Cowling, and H. J. Wilkerson, "Fundamental Study in Low-Density Gas Dynamics." Mechanical and Aerospace Engineering Research Report AE-67-023-3, University of Tennessee, November 1967.

13. Milligan, M. W., and H. J. Wilkerson, "Fundamental Study in Low-Density Gas Dynamics." Mechanical and Aerospace Engineering Research Report AE-68-023-4, University of Tennessee, December 1968.

14. Milligan, M. W., P. W. Cowling, and H. J. Wilkerson, "Rarefied Gas Flow Through Annuli." American Institute of Aeronautics and Astronautics Journal, Vol. 6, No. 5, May 1968, pp. 914-916.

15. Boon, E. F., and S. E. Tal, "Hydrodynamische Dichtung fur rotierende Wellen." Chemie-Ing-Technik, Vol. 31, No. 3, January 31, 1959, pp. 202-212.

16. Stair, W. K., "Analysis of the Viscoseal-Part 1, The Concentric Laminar Case." Mechanical and Aerospace Engineering Research Report ME-65-587-2, The University of Tennessee, January 1965.

17. Stair, W. K., "Theoretical and Experimental Studies of Visco-Type Shaft Seals." Mechanical and Aerospace Engineering Research Report ME 65-587-4, University of Tennessee, October 1965.

18. Stair, W. K., "Theoretical and Experimental Studies of Visco-Type Shaft Seals." Mechanical and Aerospace Engineering Research Report ME 66-587-5, The University of Tennessee, April 1966.

19. Stair, W. K., "Analysis of the Viscoseal, Part II, The Concentric Turbulent Case." Mechanical and Aerospace Engineering Research Report ME 66-587-7, The University of Tennessee, June 1966.

20. Kennard, E. H., Kinetic Theory of Gases. New York: McGraw-Hill Book Company, Inc., 1938.

21. Present, R. D., Kinetic Theory of Gases. New York: McGraw-Hill Book Company, Inc., 1958.

22. Fryer, G. M., "A Theory of Gas Flow Through Capillary Tubes," Proceedings Royal Society, Vol. A293, August 9, 1966, pp. 329-341.

23. Pollard, W. G. and R. D. Present, "On Gaseous Self-Diffusion in Long Capillary Tubes." Physical Review, Vol. 73, 1948, pp. 762-774.

24. Knudsen, M.,"Die Gesetze der Molekular-stromung und der inneren Reiburg-Sstromung der Gase durch Rohren," Ann. Physik, Vol. 28, 1909, pp. 75-130.

25. Lund, L. M. and A. S. Berman, "Flow and Self-Diffusion of Gases in Capillaries, Parts I and II." Journal of Applied Physics, Vol. 37, No. 6, May 1966, pp. 2489-2508.

26. Dushman, S., Scientific Foundations of Vacuum Techniques. New York: John Wiley and Sons, Inc., 1949.

27. Wilkerson, H. J.,"Experimental Investigation of Slip Flow Behavior in Constant and Varying Area Passages." Master's Thesis, The University of Tennessee, Knoxville, Tennessee, 1963.

28. Milligan, M. W. and K. E. Patterson, "Rarefied Gas Flow Through Long Square Tubes." Personal Correspondence, June 1970. (Paper submitted for presentation to 1970 Winter Annual Meeting of the American Society of Mechanical Engineers).

29. King, A. E., "A Holweck Type Molecular Vacuum Pump Used as a Shaft Seal for Alkali Metal Vapors." Report No. WAED 63-10E, Westinghouse Aerospace Electrical Div., Lima, Ohio, October 1963.

30. King, A. E., Personal correspondence, May 26, 1969.

31. Luttrull, L. H., "A Study of Convective Inertia Effects and Methods of Controlling Gas Ingestion in Large Diameter Viscoseals." Master's Thesis, The University of Tennessee, Knoxville, Tennessee, March 1970.

32. Ketola, H. N. and J. M. McGrew, "Turbulent Operation of the Visco Seal." ASLE Transactions, Vol. 10, 1967, pp. 256-272.

33. Cowling, P. W. and T. C. Swicegood, "Free Molecular Flow Through a Long Groove." Unpublished, The University of Tennessee, Knoxville, Tennessee, personal correspondence, June 1969.

APPENDICES

APPENDIX A

GROOVE SELF DIFFUSION

As stated in Chapter II, the diffusive flow in the shaft groove was
obtained by considering this flow to be that of a long groove of rectangular
cross section. This considers the helical groove to be unwrapped and
neglects any curvature effects. Thus this section presents the self-
diffusion flow through a long, straight, rectangular groove. The
development of this technique is patterned after the work of Weber [9]
and was primarily done by Cowling and Swicegood [33].

Consider the long groove of rectangular cross section of Figure 12.
Let dS' be a small element on the surface of the groove side wall and dS
be a small element in a counting plane normal to the groove axis. The
number of molecules which leave dS' per unit time in the direction of the
element is shown by Present [21] to be

$$-d^2 N_W = n\bar{V}dS' \cos \theta' \frac{d\omega}{4\pi} \; , \tag{A-1}$$

where $d\omega$ is the elemental solid angle subtended by dS at the center of dS'
and the minus sign indicates flow in the negative ξ direction. Let r be
the length of the line joining the centers of dS and dS' and θ' be the
angle between r and the normal to dS.

Of those molecules leaving dS' in the direction of dS, some will
travel the entire distance without experiencing a molecular collision.
The probability of a molecule traveling a distance r without a

68

Figure 12. Groove Geometry, Self-Diffusion Analysis.

collision is $e^{-r/\lambda}$ [21], where λ is the mean free path. Thus of the total number of molecules which leave dS' per unit time in the direction of dS, only

$$-d^2\dot{N}_W = n\overline{V}dS' \cos \theta' \, \frac{d\omega}{4\pi} \, e^{-r/\lambda} \qquad (A-2)$$

arrive there without experiencing an intermolecular collision. From geometric considerations,

$$d\omega = \frac{dS \cos \theta}{r^2}$$

$$dS = d\eta dz$$

$$\cos \theta = \frac{r^2 + \xi^2 - d^2}{2r\xi}$$

$$\cos \theta' = \frac{r^2 + (b' - \eta)^2 - f^2}{2r(b' - \eta)}$$

$$dS' = dz'd\xi.$$

Using the above equations, then Equation (A-2) may be written as

$$-d^2\dot{N}_W = \frac{n\overline{V}(d\eta dz d\xi)dz'}{16\pi r^4 \xi(b' - \eta)}[r^2 + (b' - \eta)^2 - f^2][r^2 + \xi^2 - d^2]e^{-r/\lambda}. \quad (A-3)$$

But

$$r^2 - f^2 = (b' - \eta)^2$$
$$r^2 - d^2 = \xi^2$$

Thus

$$-d^2\dot{N}_W = \frac{n\overline{V}(d\eta dz d\xi)dz'}{4\pi r^4}(b' - \eta)\xi \, e^{-r/\lambda}. \qquad (A-4)$$

Consideration will now be given to the number of molecules which pass through dS directly after experiencing a molecular collision somewhere

along r. Let $d^3\dot{N}_g$ be the number of molecules per unit time from this source of flow through dS. If $d\tau$ is an elemental volume on r, then $n\bar{V}\, d\tau/\lambda$ is the molecular collision frequency in $d\tau$ [21]. Of this number, $d\omega_2/4\pi$ leave $d\tau$ in the direction of dS where $d\omega_2$ is the solid angle subtended by dS at the center of $d\tau$. For these molecules leaving $d\tau$ in the direction of dS, the probability is $e^{-\varepsilon/\lambda}$ that they will travel to dS without a collision where ε is the distance from $d\tau$ to dS. Thus

$$-d^3\dot{N}_g = \frac{n\bar{V}}{\lambda}\, d\tau\, \frac{d\omega_2}{4\pi}\, e^{-\varepsilon/\lambda}. \tag{A-5}$$

From geometric considerations,

$$d\omega_2 = \frac{dS\cos\theta}{\varepsilon^2} = \frac{d\eta dz}{\varepsilon^2}\, \frac{\xi}{r}$$
$$d\tau = \varepsilon^2 d\omega' d\varepsilon,$$

but

$$d\omega' = \frac{dS'\cos\theta'}{r^2}$$

and

$$d\tau = \varepsilon^2\, \frac{dS'\cos\theta'}{r^2}\, d\varepsilon$$

or

$$d\tau = \frac{\varepsilon^2}{r^2}\, (dz'd\xi)\frac{(b'-\eta)}{r}\, d\varepsilon,$$

so that

$$- d^3\dot{N}_g = [\frac{n\bar{V}}{4\pi\lambda}\, \frac{(b'-\eta)\xi}{r^4}(d\eta dz d\xi)dz']\, e^{-\varepsilon/\lambda}d\varepsilon. \tag{A-6}$$

If integration is now performed for $0 \leq \varepsilon \leq r$, then the molecules passing through dS following a collision in all the sub-volumes $d\tau$ along ε can be found as

$$-d^2\dot{N}_g = \frac{\overline{V}}{4\pi\lambda} \ \frac{(b' - \eta)\xi}{r^4}(d\eta dz d\xi)dz' \int_0^r ne^{-\varepsilon/\lambda}d\varepsilon. \qquad (A-7)$$

To integrate Equation (A-7) it is necessary that the molecular density, n, be known as a function of ε. It is assumed that n can be expressed as

$$n = n_o + \xi(\frac{dn}{d\xi}), \qquad (A-8)$$

where n_o is the density in the counting plane and $(dn/d\xi)$ is taken as constant. It is further assumed that density changes in the η and z direction are negligible. Since

$$\xi = \varepsilon \cos \theta,$$

then the integral of Equation (A-7) can be evaluated as

$$\int_0^r ne^{-\varepsilon/\lambda} \ d\varepsilon = \int_0^r (n_o + \varepsilon \cos \theta \ \frac{dn}{d\xi})e^{-\varepsilon/\lambda}d\varepsilon$$

$$= \lambda(1 - e^{-r/\lambda})(n_o + \lambda \cos \theta \ \frac{dn}{d\xi}) - \lambda \cos \theta \ \frac{dn}{d\xi}re^{-r/\lambda}.$$

Thus Equation (A-7) may be written as

$$-d^2\dot{N}_g = \frac{\overline{V}}{4\pi} \ \frac{(b' - \eta)\xi}{r^4}(d\eta dz d\xi)dz' \ \{(1 - e^{-r/\lambda})(n_o + \lambda \cos \theta \ \frac{dn}{d\xi})$$

$$- \cos \theta \ \frac{dn}{d\xi} \ re^{-r/\lambda}\}. \qquad (A-9)$$

The total number of molecules passing through dS in the negative ξ direction from along the ray "r" is obtained by adding Equations (A-4) and (A-9) to obtain

$$d^2\overset{\bullet}{N}\Big|_{\xi-} = d^2\overset{\bullet}{N}_W + d^2\overset{\bullet}{N}_g \quad ,$$

which simplifies to

$$- d^2\overset{\bullet}{N}\Big|_{\xi-} = \frac{\overline{V}}{4\pi r^4}(b' - \eta)\,\xi\,(d\eta dz d\xi)dz'\,\{n_o + \lambda\cos\theta\,\frac{dn}{d\xi}(1 - e^{-r/\lambda})\},\,(A-10)$$

where

$$\cos\theta = \frac{\xi}{r} \quad .$$

Equation (A-10) expresses the total number of molecules flowing

through the counting plane in the negative ξ direction. To find the

molecules flowing through the counting plane in the positive ξ direction

it is necessary to redefine the molecular density as

$$n = n_o - \xi\,\frac{dn}{d\xi} \quad .$$

With this revision and a change of sign in Equation (A-4), the

total molecular flow in the positive ξ direction is obtained as

$$d^2\overset{\bullet}{N}\Big|_{\xi+} = \frac{\overline{V}}{4\pi r^4}(b' - \eta)\,\xi\,(d\eta dz d\xi)dz'\,\{n_o - \lambda\cos\theta\,\frac{dn}{d\xi}(1 - e^{-r/\lambda})\}. \quad (A-11)$$

The net molecular flow through the counting plane can be obtained

by adding Equations (A-10) and (A-11) and simplifying to

$$d^2\overset{\bullet}{N}_{NET} = - \frac{\overline{V}\xi^2(d\eta dz d\xi)dz'}{2\pi}\,(\frac{dn}{d\xi})\,\frac{(b' - \eta)b'\,N_{Kg}}{r^5}(1 - e^{-R/N_{Kg}}), \quad (A-12)$$

after letting

$$R = \frac{r}{b'}$$

$$N_{Kg} = \frac{\lambda}{b'} \quad .$$

Now referring to Figure 13, it is possible to write Equation (A-12)

to calculate the flow from both side walls of the groove as

Figure 13. Groove Numerical Network.

$$d^2\dot{N}_{NET} = -\frac{\overline{V}\xi^2(d\eta dz d\xi)dz'}{2\pi}\frac{d\eta}{d\xi}\{\frac{(b'-\eta)b' N_{Kg}}{r^5}(1 - e^{-R/N_{Kg}})$$

$$+ \frac{\eta b' N_{Kg}}{rr^5}(1 - e^{-RR/N_{Kg}})\} \qquad (A-13)$$

where

$$RR = rr/b'.$$

Equation (A-13) does not lend itself to closed form integration, so the solution must be obtained numerically. Equation (A-13) can be rewritten as

$$d^2\dot{N}_{NET} = -\frac{\overline{V}\xi^2(\Delta\eta\Delta z\Delta\xi)\Delta z'}{2\pi}\frac{d\eta}{dz}N_{Kg}\{\frac{(b'-\eta)b'}{r^5}(1 - e^{-R/N_{Kg}})$$

$$+ \frac{\eta b'}{rr^5}(1 - e^{-RR/N_{Kg}})\} , \qquad (A-14)$$

where

$$r = [\xi^2 + (b'-\eta)^2 + (z'-z)^2]^{1/2}$$

$$rr = [\xi^2 + \eta^2 + (z'-z)^2]^{1/2}$$

Computation Procedure

The molecular flow indicated by Equation (A-14) was evaluated in the following manner. As shown in Figure 13, let each differential flow, $DFLOW_{jk}$, from the two side walls to an "i" element be summed along a constant "j" row for $1 \leq k \leq N$, and let $RFLOW_{ij}$ represent that sum. So

$$RFLOW_{ij} = \sum_{k=1}^{N} DFLOW_{jk}.$$

Then the total flow to an "i" element is given by

$$FLOW_{ij} = \sum_{j=1}^{M} RFLOW_{ij} \quad (i = constant).$$

The next step in the solution is to calculate the total flow to each differential "i" element along the bottom row, (i,1). Because of symmetry, it is only necessary to compute this flow over one-half of the flow channel width.

Next, to reduce the computer execution time, certain geometrical similarities can be found to reduce the number of calculations. For example, if any $FLOW_{ij}$ could be found by adding and subtracting certain $RFLOW_{ij}$ to $RFLOW_{i1}$, then the number of calculations can be drastically reduced. Figure 14 illustrates a method for determining this similarity.

From Figures 13, page 74, and 14 note that $FLOW_{i2}$ is very similar to $FLOW_{i1}$. In fact, the only difference is the dotted RFLOW's shown. Thus it can be seen that

$$FLOW_{i2} = FLOW_{i1} + RFLOW_{i2} - RFLOW_{iM}.$$

In a more general sense, since $FLOW_{i3}$ may be obtained from $FLOW_{i2}$ in a similar manner, then

$$FLOW_{ij} = FLOW_{i,j-1} + FLOW_{i,j} - RFLOW_{i,M + 2 - j}.$$

Now this $FLOW_{ij}$ can be summed over each element for one quadrant of the channel cross-section and multiplied by 4 to obtain the total diffusive flow from the channel side walls.

For a channel of square cross-section with a uniform molecular concentration across the channel, the flow from the bottom and top walls is the same as the flow from the groove side walls. Thus the total diffusion flow through a square groove is given by

$$\overset{\circ}{N} = 8 \sum_{i=1}^{L/2} \left(\sum_{j=1}^{M/2} FLOW_{ij} \right). \tag{A-15}$$
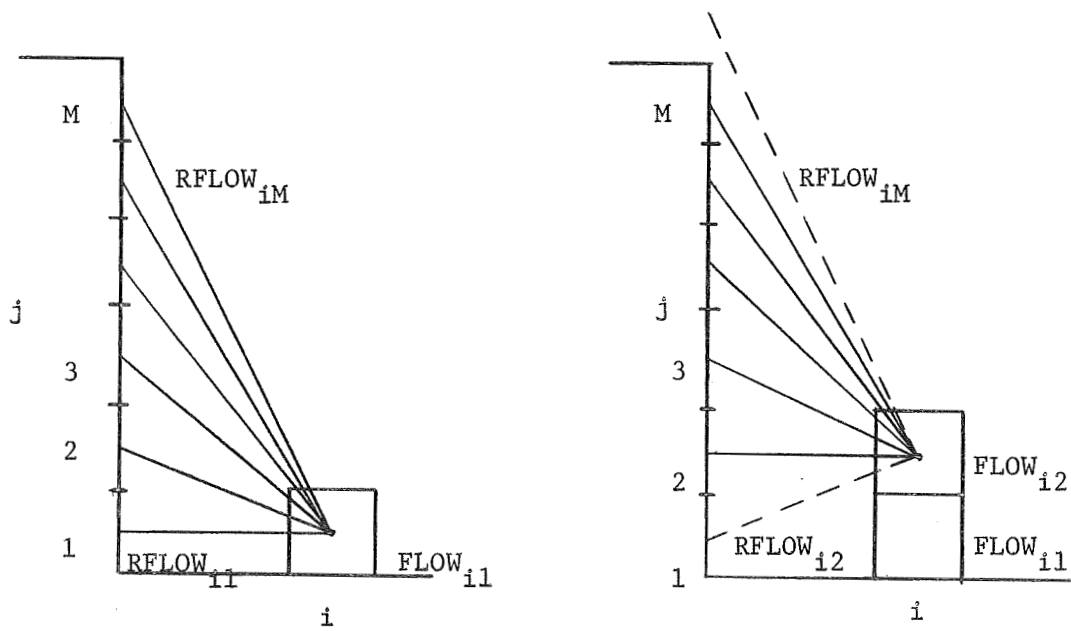
Figure 14.   Numerical Computation Similarities.

Commentary

The solution for the self-diffusion flow presented in this section has been recently utilized by Milligan and Patterson [28] in a study of rarefied gas flow through long square tubes. Their experimental results substantiate the diffusive analysis presented.

APPENDIX B

KING'S ANALYSIS OF THE RAREFIED-GAS VISCOSEAL

The analysis of the rarefied-gas viscoseal by King [6] is unique
in its manner of treatment of the viscous induced flow in the grooves
superimposed with the pressure induced flows in both the grooves and
the annular clearance space. The rotor induced flow in the grooves
is determined by considering viscous flow without a pressure gradient
in a rectangular channel with one wall moving at the peripheral speed
of the rotor. The pressure induced leakage flows of the grooves and
the annular space are established using the Poiseuille viscous tube
flow equation modified with slip boundary conditions after having
assumed these flows could be represented by use of the hydraulic radius,
r_H, in the tube flow equation.

King evaluates the net leakage mass flow rate in the seal as

$$\overset{\circ}{m}_{NET} = N_s \overset{\bullet}{m}_D + \overset{\bullet}{m}_d - N_s \overset{\circ}{m}_I, \qquad (B-1)$$

where

$\quad \overset{\circ}{m}_D$ = pressure induced mass flow in a groove

$\quad \overset{\circ}{m}_d$ = pressure induced mass flow in the annulus

$\quad \overset{\circ}{m}_I$ = rotor induced mass flow in a groove

$\quad N_s$ = number of grooves

The terms are evaluated in the following manner.

Groove Flow

King assumes that Poiseuille flow in a tube when modified using
slip boundary conditions at the walls is applicable to the pressure

induced flow through use of the hydraulic radius in place of the tube radius. The Poiseuille solution for tube flow is given by Kennard [20] as

$$\dot{m}_D = \frac{\rho \pi r_t^4}{8\mu} \frac{dP}{d\ell} (1 + 4 \frac{\zeta}{r_t}),$$ (B-2)

where ζ is the coefficient of slip as defined by Kennard in evaluating the slip velocity relative to the wall as

$$u_w = - \zeta \frac{du}{dr} .$$

The coefficient of slip is taken from [26] as

$$\zeta = (\text{constant}) \lambda = 1.375 \lambda.$$

Using the perfect gas equation of state for the density, Equation (B-2) is rewritten in terms of the cross sectional area and the hydraulic radius as

$$\dot{m}_D = \frac{MAr_H^2}{8R_o T\mu} P \frac{dP}{d\ell} (1 + \frac{5.5 \lambda}{r_H}).$$ (B-3)

Annular Clearance Flow

Similarly to the pressure induced flow treatment in the groove, King treats the annulus flow by a modified form of the Poiseuille flow solution. The annulus flow, $\dot{m}_d$, will differ from the groove Equation (B-3) only in terms of the hydraulic radius, the cross sectional area, and the pressure gradient. The ratio for the two flows was defined for N_s parallel grooves as

$$\frac{\dot{m}_d}{N_s \dot{m}_D} = \delta$$ (B-4)

or

$$\delta = \frac{A'(r_{H'})^2(1 + \frac{4\zeta}{r_H'})P' \frac{dP'}{dL}}{(N_s)A(r_H)^2(1 + \frac{4\zeta}{r_H})P \frac{dP}{d\ell}} , \qquad \text{(B-5)}$$

where the primes designate the annulus terms. King considers the pressure

at either end of the grooves and across n_ℓ thread lands in the test

section must be equal so that

$$\int_0^\ell P \frac{dP}{d\ell} d\ell = \int_0^{a(n_\ell)} P' \frac{dP'}{dL} dL,$$

which he uses to approximate that

$$\frac{P' \frac{dP'}{dL}}{P \frac{dP}{d\ell}} = \frac{\ell}{a(n_\ell)} ,$$

where "a" is the axial land width as shown in Figure 2, page 10. Thus

$$\delta = \frac{A'(r_H')^2(1 + \frac{4\zeta}{r_H'})\ell}{(N_s)A(r_H)^2(1 + \frac{4\zeta}{r_H})a(n_\ell)} \qquad \text{(B-6)}$$

The terms of Equation (B-6) were evaluated as follows:

$$A' = \pi(D + c)c$$

$$r_{H'} = \frac{2 \cdot \text{cross sectional area}}{\text{wetted parameter}} = c$$

$$\ell = \frac{L}{\sin \alpha}$$

$$A = hb'$$

$$r_H = \frac{hb'}{(h + b')}$$

$$n_\ell = \frac{L}{(b' + a)}$$

$$N_K = \frac{\lambda}{c}$$

where b' is the groove width normal to the groove walls and is related

to the groove axial width b of Figure 2, page 10, by

b' = b cos α.

Using the above equations,

$$\delta = \frac{\pi(D + c)c^3(h + b')^2(b' + a)[1 + 5.5\ N_K]}{N_s\ \sin\ \alpha(hb')^3 a\ [1 + 5.5\ N_K\frac{c(h + b')}{hb'}]} \qquad (B-7)$$

Rotor Induced Flow

In his evaluation of the rotor induced flow King considers only

the viscous terms of the Navier-Stokes equations and selects for his

model

$$\frac{\partial^2 u}{\partial \eta^2} + \frac{\partial^2 u}{\partial z^2} = 0. \qquad (B-8)$$

This equation is solved subject to the boundary conditions, reference

Figure 2, page 10,

u = 0 at η = 0

u = 0 at η = b'

u = 0 at z = h + c

u = U cos α at z = 0

It should be noted that these are continuum type boundary conditions

and do not include any rarefication effects. Using separation of

variable techniques, King obtains the groove velocity distribution and

integrates over the groove area to obtain the average rotor induced

velocity

$$\bar{u} = \frac{8U\ \cos\ \alpha\ b'}{(h + c)\ \pi^3}\ \sum_{n\ =\ 0}^{\infty}\ \frac{1}{(2n + 1)^3}\ \{\frac{\cosh\ [(2n + 1)\ \frac{\pi(h + c)}{b'}] - 1}{\sinh\ [(2n + 1)\ \frac{\pi(h + c)}{b'}]}\},$$

or

$$\bar{u} = \frac{8U \cos \alpha \ b'}{(h + c) \ \pi^3}[SUM \ (K)].$$ (B-9)

The rotor induced flow is thusly obtained as

$$\overset{\circ}{m}_I = \rho A \bar{u} = \frac{PM}{R_o T} A \bar{u} \ .$$ (B-10)

Net Flow

The net leakage flow is summated in Equation (B-1) and, using

Equations (B-2), (B-4) and (B-10), may be expressed as

$$\overset{\circ}{m}_{NET} = (1 + \delta) \frac{AMr_H^2 N_s}{8R_o T \mu} \ [1 + \frac{5.5\lambda}{r_H}] \ P \frac{dP}{d\ell} - \frac{N_s AM\bar{u}}{R_o T} P.$$ (B-11)

To find the maximum pressure differential across the seal, King sets

the net mass flow to zero. Then letting

$$\frac{dP}{d\ell} \overset{\sim}{\sim} \frac{\Delta P}{\ell} = \frac{\Delta P \sin \alpha}{L} \ ,$$

$$P_{max} = \frac{8\bar{u}L\mu}{\sin \ (1 + \delta)r_H^2 \ [1 + \frac{5.5\lambda}{r_H}]} \ .$$ (B-12)

The sealing coefficient as defined in Equation (2-29) may now be

evaluated after substituting for the hydraulic radius, r_H, as

$$\Lambda = \frac{3\pi^2 \tan \alpha(h + c)h^2b' \ (1 + \delta)[1 + \frac{5.5 \ N_K c \ (h + b')}{hb'}]}{32 \ c^2(h + b')^2[SUM(K)]} \ .$$ (B-13)

Commentary

The sealing coefficient as computed using Equation (B-13) is shown

on Figure 15 together with representative examples of King's experimental
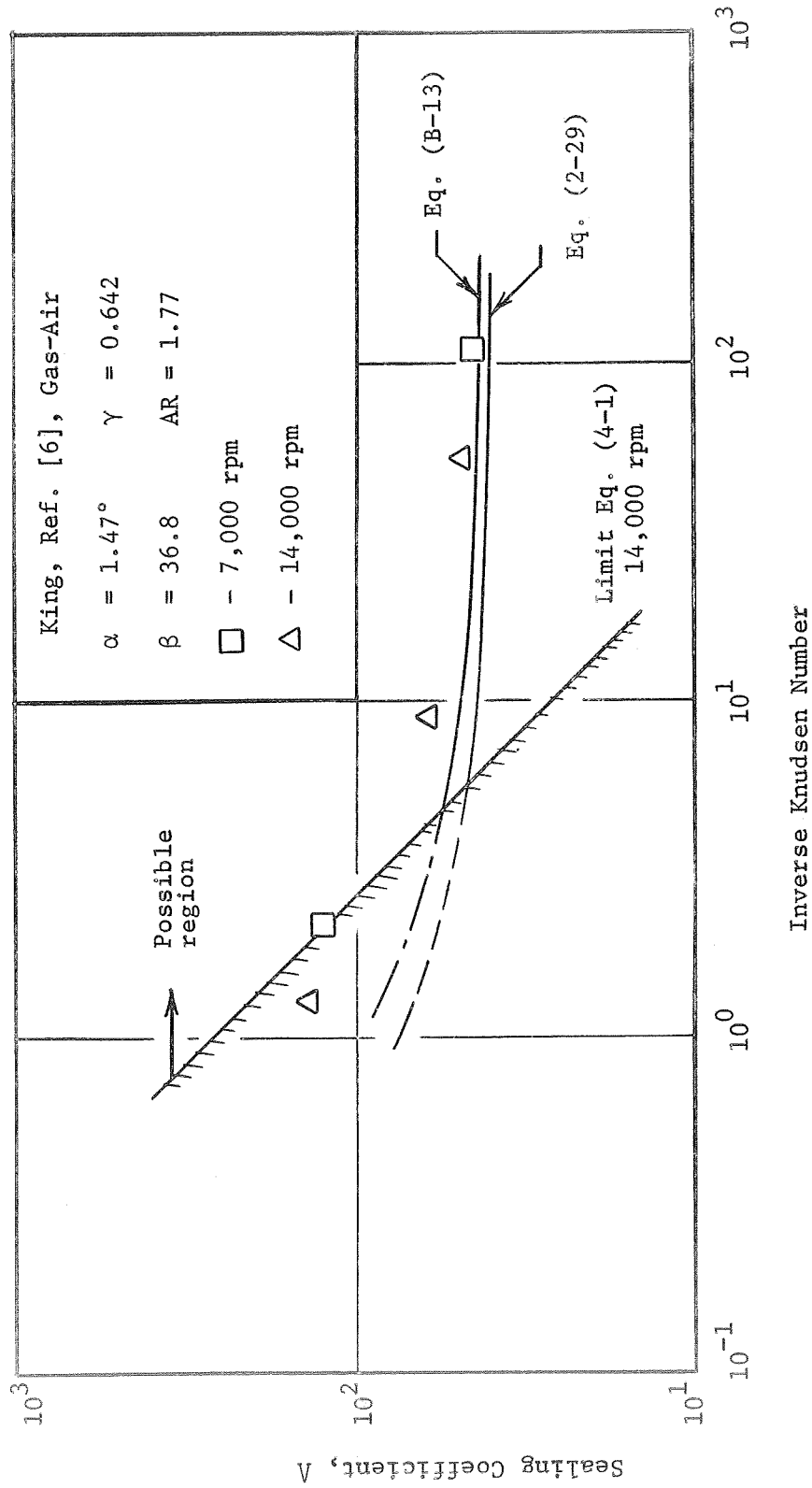
Figure 15. Sealing Coefficient Versus Inverse Knudsen Number – King's Analysis.

data and the solution of Equation (2-29). As may be observed, the trends and both theories are remarkably similar and both solutions have significant deviations from the data. A primary motivation for the close examination of King's efforts was the excellent agreement between theory and experiment shown in References [6] and [29]. Numerous efforts to duplicate this agreement have been unsuccessful. The reader is cautioned that numerous errors are present in both References [6] and [29] of King's work and were confirmed generally but not specifically by the personal correspondence of the author [30]. To the best of the author's knowledge the equations are correct as presented herein.

APPENDIX C

CONTINUUM INVESTIGATION OF THE EXPERIMENTAL

RAREFIED-GAS VISCOSEAL NO. 1

In order to obtain experimental data over the widest possible rarefication range, it was elected to conduct a continuum sealing coefficient investigation. Although this was not within the original research scope, it was felt that these experiments would add supporting evidence for the rarefied tests. This goal was accomplished by the data shown on Figure 7, page 51. In the process of obtaining this information, certain characteristics of a continuum viscoseal were uncovered that have not been previously reported and are contained in this appendix.

The continuum sealing coefficient experiments were conducted by removing the graphite ring seal and the vacuum pump connections as shown on Figure 3, page 29, in order to permit atmospheric pressure conditions to exist at the downstream location. The high pressure end of the viscoseal test section was maintained as a sealed cavity and was pumped to an equilibrium pressure above atmospheric during the dynamic tests. The pressure drop across the viscoseal test section was measured using an inclined manometer. Shaft speed was measured using an electronic counter as discussed in Chapter III.

Figure 16 presents the sealing coefficient data versus the clearance Reynolds number where

$$Re_c = \frac{\rho U c}{\mu} . \tag{C-1}$$

Figure 16. Continuum Sealing Coefficient Versus Clearance Reynolds Number, Seal No. 1.
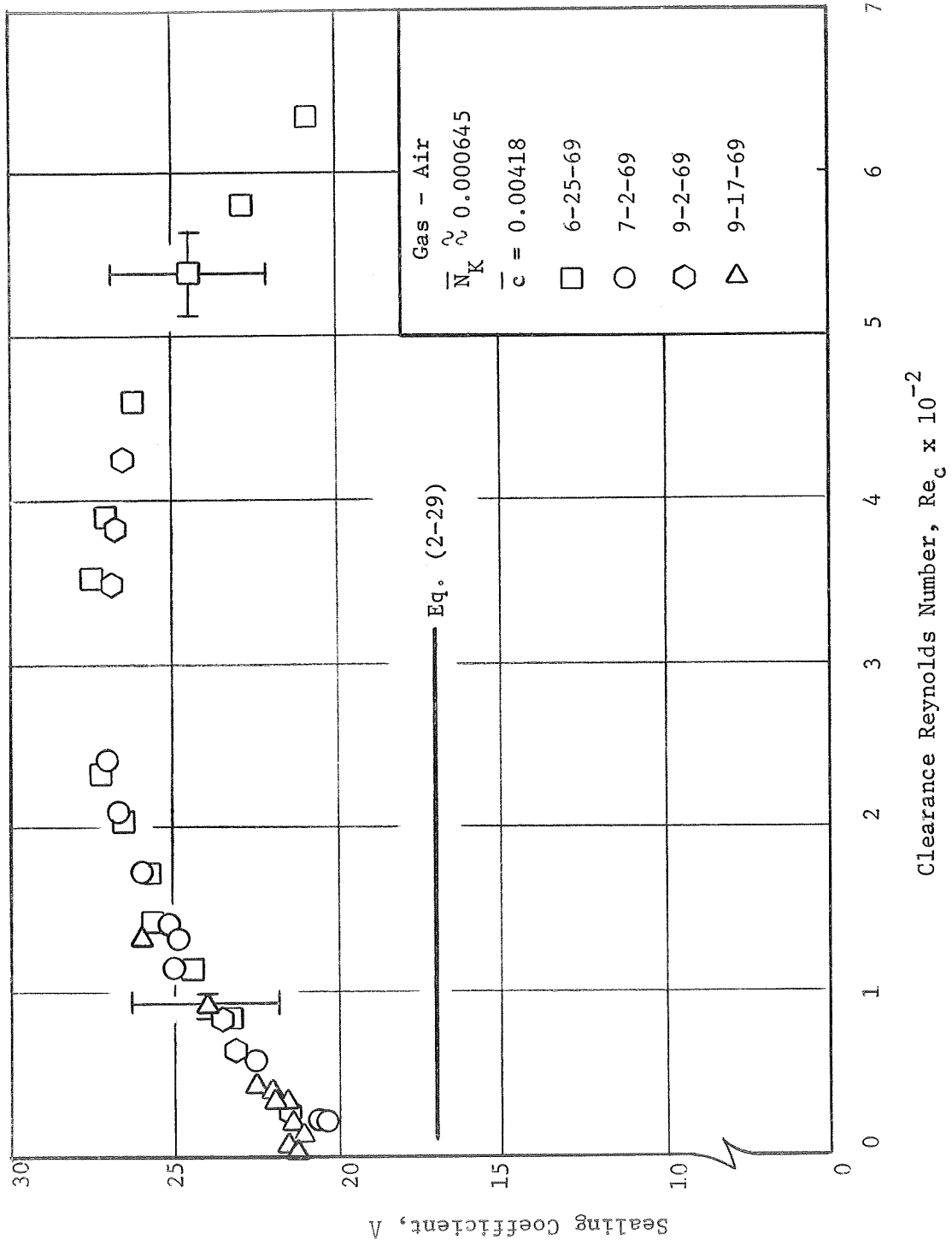
The theoretical solution of the developed rarefied Equation (2-29),
which reduces to the Boon and Tal solution of Equation (2-30) for
continuum conditions, is shown. It is observed that the predictions
of the equation are optimistic in comparison to the experimental data.
The experimental sealing coefficient data has a rather bell shape with
the maximum value of Λ, minimum sealing performance, occurring at a
Reynolds number of approximately 350. The sealing coefficient decreases
with increases in Reynolds number above 350 due to what Stair [17]
attributes to the onset of turbulence. Luttrell [31] discusses inertia
effects as the source of this occurrence. The value of 350 is within
the "transition" values of 300-600 determined by Stair in his experiments
in which water was the sealant but is somewhat above the value of 180
of Figure 9, page 58, determined by Hodgson and Milligan [7] using air.
Luttrell [31] reports that the onset of this transition occurrence is
delayed with decrease in the groove aspect ratio. This is substantiated
by comparing the transition value of Hodgson and Milligan's data for
an aspect ratio of 11.9 with that reported here which has an aspect
ratio of essentially unity.

The major difference in the trends of the continuum sealing data
from that previously reported is in the lower Reynolds number range below
350 where the sealing coefficient decreases with decreased Reynolds
number. A number of investigators [7, 17, 18, 19, and 31] have reported
excellent agreement in this range with the Boon and Tal theory which
predicts a constant value of sealing coefficient. Because of this
departure from "anticipated" results additional investigations using
completely different and independent methods for measuring the seal ΔP

and shaft speed were conducted and the original data confirmed.

Figure 17 shows a plot of ΔP across the seal versus shaft speed. For all other sealing coefficient variables held constant, the ΔP must increase linearly with shaft speed for Λ to remain constant. It may be observed that the major departure from a linear relation occurs at very low shaft speeds. For this reason, Figure 18 is included to enlarge the speed range below 10,000 rpm. It is this small departure from linearity that produces the pronounced changes in the sealing coefficient values in this range. A close examination of Luttrell's Figure 21 of Reference [31] and of Stair's Figure 21 of Reference [19] and Figures 2, 4, and 7 of Reference [18] show slight evidences similar to that reported here. The data of Ketola and McGrew [32] also show similar trends. These references have either omitted or made minimum mention of this aspect.

As previously stated, the general level of the sealing coefficient data is above the predictions of Equation (2-29) and does not show the degree of correlation reported in references [7, 17, 18, and 19] between theory and experiment. This may be partially due to the fact that in the evaluation of the sealing coefficient data that the true $\Delta P/L$ drop across the viscoseal section was used. Stair in References [18 and 19] measured the pressure distribution along the seal length and utilized dP/dL based on the best plot of the pressure distribution exclusive of the upstream pressure. Stair reports on page 5 of Reference [18] that the observed actual pressure differences, ΔP, were approximately 88 to 92 percent of the theoretical values. If similar ratios were applied to the experimental results reported herein,

Figure 17. Seal Differential Pressure Versus Shaft Speed, Seal No. 1
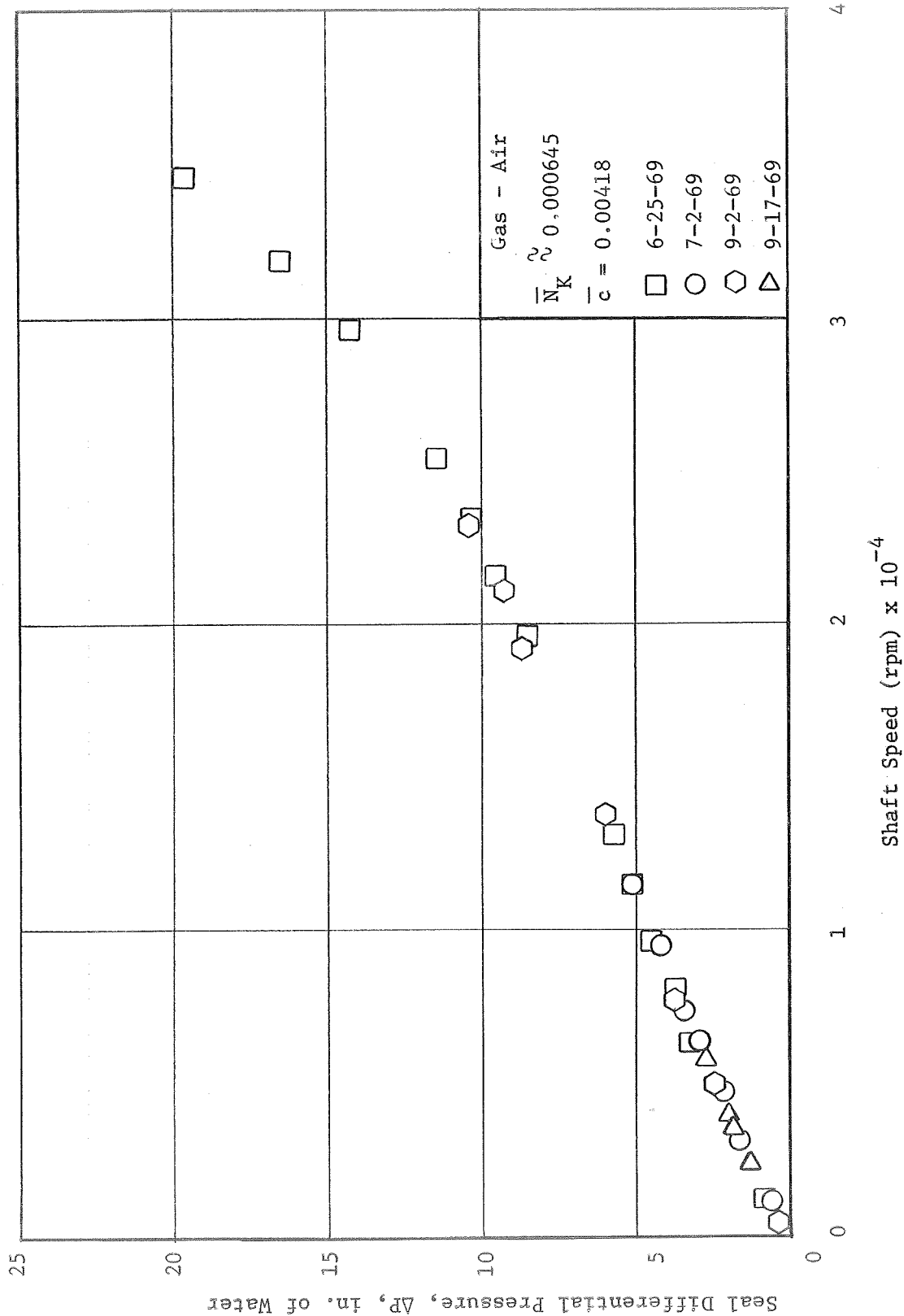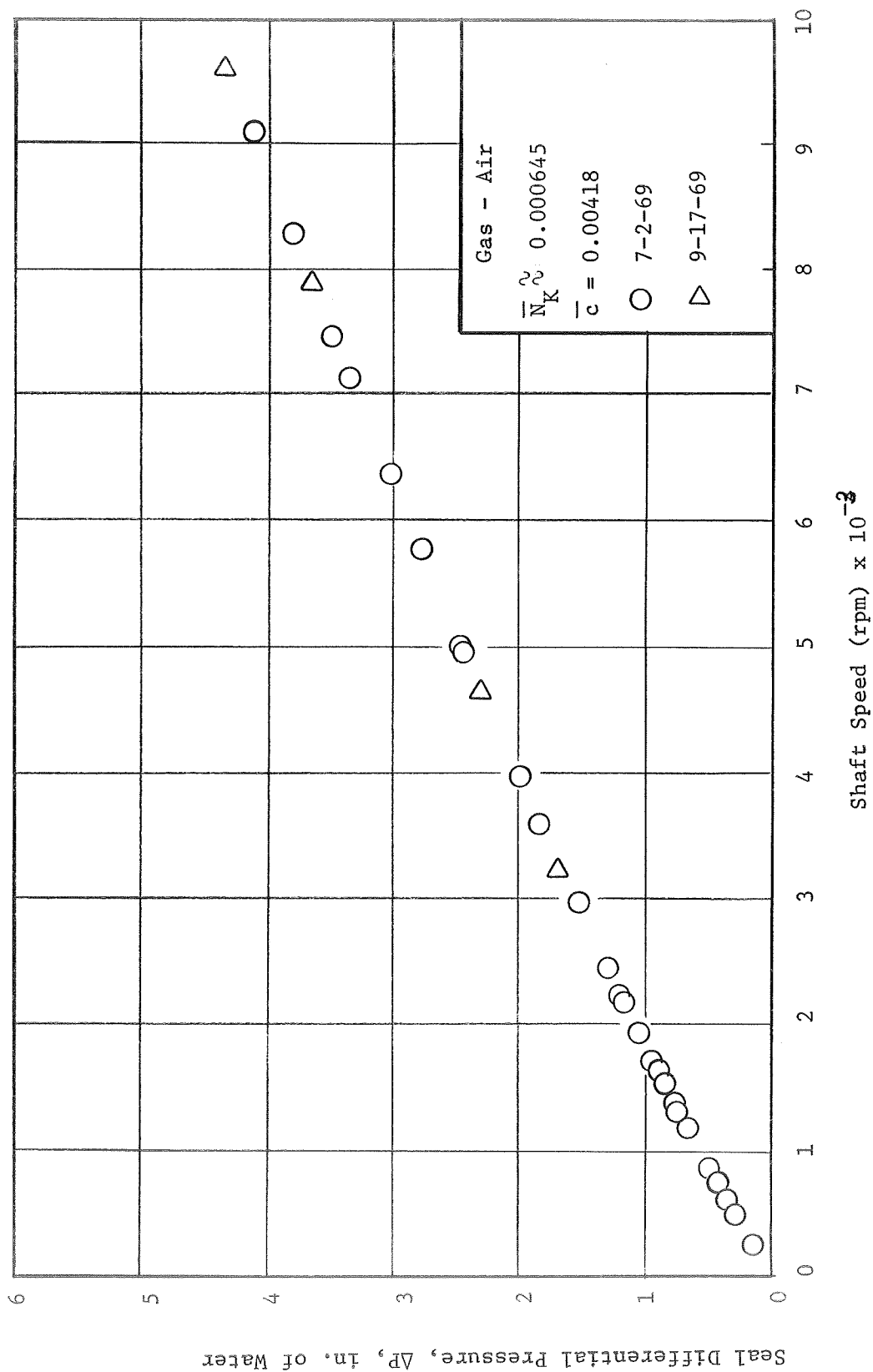
Figure 18.   Seal Differential Pressure Versus Shaft Speed, Seal No. 1

considerable improvement in the correlation between theory and experiment would result. There are many other factors which may account for the differences including vibrations, shaft runout, eccentricity, misalignment, end effects, and experimental uncertainty. After consideration of each of these, however, it is the writer's opinion that the primary reason is due to the absence of boundary conditions on the groove side walls in the theoretical model when dealing with grooves of very low aspect ratio. Luttrell's data for grooves of lower aspect ratios [31] also show decreases in sealing performance in comparison to the Boon and Tal theory similar to that reported here. The previous investigations of references [7, 18, and 19] that have reported very good agreement between experiment and the Boon and Tal theory have been for grooves of much higher aspect ratios.

The results of this continuum investigation of sealing coefficient suggest the need for caution when applying the Boon and Tal model to viscoseal designs having low aspect ratio grooves. A similar conclusion was reached in Chapter IV based on the net leakage investigations. This portion of the study has also indicated the general need for additional experimental investigations in the low Reynolds number regime with emphasis on low aspect ratio grooves.

It may be noted that the absence of experimental data near a clearance Reynolds number of 300, or a shaft speed of 16,000 rpm, is due to the existence of a critical shaft speed at this condition.

APPENDIX D

CONSTANTS AND CONVERSION FACTORS

Argon Constants

$M = 39.944$

$m = 66.2 \times 10^{-24}$ gm/molecule

$\mu = 2.258 \times 10^{-4}$ gm/cm sec $\left.\begin{array}{l} \\ \\ \end{array}\right\}$ $T = 297°K$

$\quad\quad 1.262 \times 10^{-6}$ lbm/in sec

Fundamental Constants

$K = 1.3804 \times 10^{-16}$ dyne-cm/molecule-°K

$R_o = 8.3166 \times 10^{7}$ dyne-cm/gm·mole-°K

Conversion Factors

1 dyne/cm^2 = 0.7501 μhg

APPENDIX E

TABULATED EXPERIMENTAL REDUCED DATA FOR

RAREFIED VISCOSEAL NO. 1

TABLE IV

NET LEAKAGE REDUCED DATA FOR SEAL NO. 1, ZERO RPM

Data Point No.	P_T µhg	P_b µhg	$1/N_K$	$\dot{N}/\Delta P$ x 10^{-14}
1	16,800	7,230	24.68	18.16
2	19,150	7,705	27.57	20.30
3	21,400	8,155	30.32	21.60
4	22,600	8,430	31.87	22.08
5	17,000	7,465	25.09	17.45
6	12,150	565	13.05	10.60
7	9,370	538	10.15	9.06
8	8,100	522	8.84	8.24
9	6,850	512	7.54	7.28
10	5,450	500	6.10	6.34
11	4,180	495	4.79	5.50
12	4,200	490	4.80	5.46
13	2,950	487	3.52	4.65
14	1,870	482	2.41	3.81
15	13,800	1,250	15.40	11.31
16	1,740	255	2.10	3.47
17	1,700	260	2.01	3.60
18	1,720	275	2.05	3.59
19	752	227	1.00	3.23
20	428	132	0.57	3.02
21	318	129	0.46	2.83
22	251	131	0.39	2.40
23	216	131	0.36	2.48
24	4,000	131	4.23	5.26
25	2,320	172	2.55	4.15
26	1,460	166	1.66	3.46
27	1,025	168	1.22	3.30
28	600	172	0.77	2.77
29	475	131	0.62	3.20

TABLE V

NET LEAKAGE REDUCED DATA FOR SEAL NO. 1, DYNAMIC SPEEDS

Data Point No.	P_T µhg	P_b µhg	$1/N_K$	$\dot{N}/\Delta P$ $\times 10^{-14}$	c in. $\times 10^3$
		10,000 rpm, $\bar{c} \times 10^3 = 3.87$ in., $\bar{r}_p = 146.4$			
1	9,380	335	8.83	0.558	3.81
2	6,410	60	6.03	0.117	3.80
3	13,200	86	12.9	1.50	3.90
4	16,700	93	15.9	2.74	3.87
5	28,700	150	27.5	7.80	3.87
6	32,500	166	30.9	9.80	3.87
7	8,050	64	7.78	0.237	3.91
10	31,000	233	30.7	10.15	4.01
		5,000 rpm, $\bar{c} \times 10^3 = 3.85$ in., $\bar{r}_p = 176.6$			
11	16,800	63	16.6	7.29	4.01
12	11,200	42	10.6	4.14	3.84
13	7,900	33	7.18	2.61	3.69
14	6,150	30	5.88	1.88	3.88
15	3,700	27	3.51	0.953	3.84
16	1,950	26	2.03	0.540	3.76
17	1,250	29	1.32	0.290	3.94
		30,000 rpm, $\bar{c} \times 10^3 = 3.29$ in., $\bar{r}_p = 807$			
18	44,000	53	36.0	0.451	3.33
19	49,900	64	40.9	1.36	3.33
20	39,800	49	31.4	0.038	3.20

TABLE VI

RAREFIED SEALING COEFFICIENT REDUCED DATA FOR SEAL NO. 1

Data Point No.	P_T µhg	P_b µhg	$1/N_K$	Λ	Re_c	c in. x 10^3
		10,000 rpm, $\bar{c}$ x 10^3 = 3.98 in.				
SP1	7,160	267	7.47	40.2	1.01	4.18
SP2	9,860	1,220	11.1	31.8	1.49	4.15
SP3	5,200	275	5.01	68.3	0.67	3.80
SP9	14,200	3,495	16.9	28.3	2.28	3.98
SP10	17,200	6,605	22.6	29.3	3.02	3.94
SP13	19,200	7,755	25.5	27.1	3.42	3.94
SP14	8,700	44	8.29	36.4	1.10	3.91
SP19	7,350	44	6.96	43.1	0.93	3.91
		5,000 rpm, $\bar{c}$ x 10^3 = 3.99 in.				
SP4	2,600	166	2.69	60.8	0.18	4.04
SP5	11,000	4,730	15.6	22.5	1.03	4.11
SP6	3,880	176	3.94	39.9	0.26	4.04
SP7	3,160	407	3.47	53.7	0.23	4.04
SP15	2,850	50	2.72	56.7	0.18	3.90
SP16	13,300	8,245	20.6	30.2	1.39	3.98
SP17	3,920	146	3.69	46.5	0.25	3.73
SP18	4,400	382	4.65	36.6	0.31	4.04
SP20*	4,200	559	4.47	43.6	0.30	3.90
SP21*	7,000	1,835	8.44	29.6	0.57	3.97
SP22*	7,550	1,710	8.94	25.5	0.60	4.01
SP23*	13,100	8,145	20.7	29.8	1.39	4.04

*Argon blanket on graphite ring seal.

Data Point No.	P_T µhg	P_b µhg	$1/N_K$	Λ	Re_c	c in. x 10^3
		30,000 rpm, $\bar{c}$ x 10^3 = 3.41 in.				
SP11	35,200	104	29.3	34.7	11.8	3.44
SP12	38,100	68	30.9	33.5	12.5	3.37